Nanoscale

REVIEW

View Article Online
View Journal

Cite this: DOI: 10.1039/d5nr04810a

Toxic element-free quantum dots as nanocarriers in drug delivery: the role of functional ligands in hybrid systems development

Patrycja Kowalik, [a] Piotr Bujak *[b] and Adam Pron *[b]

Among the numerous types of nanocarrier which can be used as drug delivery systems, such as polymeric, solid lipid and metal nanoparticles, colloidal nanocrystals of inorganic semiconductors (quantum dots, QDs) play an important role. QDs are, in fact, hybrid nanoobjects consisting of an inorganic core capped with organic ligands inducing their colloidal stability. This structure endows QDs with properties unmatched by other types of nanomaterial. For example, hydrophobic nanocrystals can be rendered hydrophilic by exchanging the primary hydrophobic ligands for hydrophilic ones, yielding colloidally stable aqueous dispersions. The introduced ligands can be further functionalized by covalent grafting of drug molecules or by exploiting non-covalent interactions between the drug and the surfacial ligand. Other bioactive molecules can also be attached to the surface of nanocrystals, so-called "*targeting ligands*", ensuring efficient transport of drugs to their final destination. Over the last 15 years, a number of synthetic procedures have been developed for the preparation of nanocrystals free of toxic elements that emit not only in the NIR-I biological window (650–950 nm), but also in the NIR-II window (1000–1400 nm). More recently, carbon dots (CDs) have emerged as a class of nanomaterials that, in certain aspects such as size range and size-dependent photoluminescence, exhibit strong similarities to inorganic semiconductor quantum dots (QDs). The aim of this short review is to critically evaluate these two types of nanomaterial, with particular emphasis on their functionalization for application as drug nanocarriers.

Received 13th November 2025,
Accepted 29th April 2026

DOI: 10.1039/d5nr04810a

rsc.li/nanoscale

1. Introduction

The original research on inorganic semiconductor nanocrystals and the quantum confinement phenomenon related to them dates back to the 1980s when Ekimov and Onushchenko[1] and Brus[2] observed a clear effect of the size of the "crystals" on their optical properties. However, the widespread interest in this type of nanomaterial started in 1993, following the appearance of a publication by Moungi Bawendi *et al.* which described the first method of the preparation of cadmium chalcogenides nanocrystals (CdE, E = S, Se, Te) of narrow size dispersion.[3] The obtained *quasi*-monodispersed nanocrystals exhibited a distinct quantum confinement effect manifested, among others, by their size-dependent photoluminescence color. For this reason, they are referred to as "quantum dots" (QDs), a term that emphasizes their quantum electronic properties and their small dimensions. This discovery was followed by an essentially exponential growth of articles devoted to various aspects of the physics, chemistry and technological applications of these nanomaterials. For their work on quantum dots, Ekimov, Brus, and Bawendi were awarded the Nobel Prize in Chemistry in 2023.[4]

Two additional pioneering papers from the early stages of quantum dot research should be mentioned here, both published by Alivisatos's group. They were devoted to two distinctly different applications. The first one described the use of CdSe QDs as components of light-emitting diodes (LEDs),[5] whereas in the second, applications of QDs in bioimaging were discussed.[6,7] Since then, these abovementioned domains of QD applications have constantly been developing through formulating new research concepts. In the case of biological and biomedical applications, the toxicity of cadmium turned out to be a serious problem since CdSe nanocrystals were commonly used at that time. In particular, it was shown that the selenide ions of these nanocrystals could undergo oxidation with the simultaneous release of free cadmium ions from the nanocrystal surface to the environment.[8,9] This phenomenon stimulated research on encapsulating CdSe nanocrystals with a shell consisting of an amphiphilic polymer. Special emphasis was placed on ensuring that this encapsulation did not significantly worsen the luminescence properties of the nanocrystals and their stability over a wide pH range.[10,11] However, this approach did not solve the toxicity problem, as demonstrated

[a]*Institute of Physical Chemistry, Polish Academy of Science, Kasprzaka 44/52, 01-224 Warsaw, Poland*
[b]*Warsaw University of Technology, Faculty of Chemistry, Noakowskiego 3, 00-664 Warsaw, Poland. E-mail: piotr.bujak@pw.edu.pl, adam.pron@pw.edu.pl*

by *in vivo* investigations involving the intravenous administration of 25 mg kg^{-1} polymer-coated core/double-shell QDs (CdSe/CdS/ZnS) to male rhesus macaques followed by the determination of their impact on the organism over a 90-day period. No toxic cadmium release or adverse histological changes in major organs were observed.

However, after 90 days, most of the nanocrystalline material accumulated in the liver, spleen, and kidneys, which could pose a risk to the organism in the long term.[12] It was therefore necessary to elaborate methods for the preparation of colloidal nanocrystals of inorganic semiconductors that did not contain toxic elements such as cadmium, lead, and mercury. Another class of QDs free of toxic elements and considered promising for biological and medical applications is represented by colloidal carbon dots, also referred to as carbon quantum dots (CDs). These luminescent carbon nanoparticles, typically ranging in size from 1 to 10 nm, have been reported to exhibit size-dependent optical properties commonly attributed to the quantum confinement effect. Owing to the development of synthetic strategies employing naturally derived carbon precursors, CDs have often been described as biogenic quantum dots.[13,14]

Another important issue related to the biomedical applications of QDs was the determination of the desired spectral ranges of their absorption and emission. This problem is closely related to the so-called "*biological spectral window*" in which the biological background absorption is the lowest. The first biological window (NIR-I) covers the spectral range of 650–950 nm. In 2009, pioneering studies emerged revealing the second biological window (NIR-II), ranging from 1000 nm to about to 1400 nm or even 1700 nm, depending on the system studied.[15,16] In the spectral range of NIR-II the absorption of photons by water molecules is slightly higher as compared to NIR-I. This is, however, overcompensated by reduced scattering on tissues and ultra-low autofluorescence, *i.e.* fluorescence resulting from fluorescent molecules naturally present in the tissues. As a result, key parameters determining the quality of the obtained images such as detection depth, resolution and sensitivity are being improved.[17,18]

The problems described above prompted a rapid growth of research aimed at obtaining nanocrystals free of toxic elements that would additionally emit light in the NIR-I or NIR-II spectral ranges. Fig. 1a shows the possible spectral ranges of the emission tuning determined for selected binary, ternary and quaternary nanocrystals of inorganic semiconductors which contain neither cadmium nor lead or mercury. These nanocrystals are presently used not only for bioimaging but also as nanocarriers for drug delivery. Tuning of their light absorption and emission is possible through strict control of their size and shape, *i.e.* by exploiting the quantum confinement effect.[2,19,20] However, a more convenient and general method for modifying optical properties is the preparation of ternary or quaternary nanocrystals, which are alloys of two or more binary semiconductors (Fig. 1b).[21,22] It should also be noted that there exists a large group of multicomponent nanocrystals whose compositions strongly deviate from those imposed by alloying. This phenomenon is also being exploited in the preparation of nanocrystals of tunable absorption and emission.[23,24]

In the design of nanocrystals emitting radiation in the NIR-I and NIR-II spectral ranges, the value of the energy gap (E_g) is crucial. This value strictly depends on the bulk energy

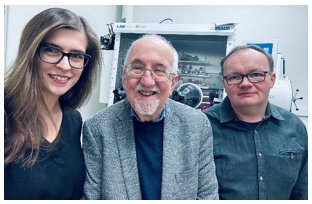

From left to right: Patrycja Kowalik, Adam Pron, and Piotr Bujak

Patrycja Kowalik obtained her MSc in Chemistry from the University of Warsaw in 2018. In the same year, she began her doctoral studies within a joint PhD program of the Warsaw University of Technology (WUT) and the University of Warsaw (UW), under the supervision of Professor Piotr Bujak (WUT) and Professor Anna Nowicka (UW). She obtained her PhD in 2023 with a dissertation devoted to the synthesis and investigation of the properties of toxic metal-free inorganic semiconductor nanocrystals. Since 2023, she has been working as a postdoctoral researcher at the Institute of Physical Chemistry of the Polish Academy of Sciences. She is a co-author of more than 20 scientific publications, a large number of which are devoted to the surface functionalization of nanocrystals for their application as drug nanocarriers.

Piotr Bujak graduated from the Silesian University of Technology (SUT) in 2004. In 2008, he received his PhD from the University of Silesia (US). His doctoral dissertation, carried out under the supervision of Professor Marek Matlęgiewicz, was devoted to the structural investigation of selected polymers using NMR spectroscopy. He subsequently joined the Faculty of Chemistry at the University of Silesia, where he developed an efficient method for the synthesis of new isoxazolines. In 2012, he accepted a position as a research associate at the Warsaw University of Technology, joining the group of Professor Adam Pron, where he initiated research on inorganic semiconductor nanocrystals. In 2019, he was promoted to the position of associate professor. He is the author and co-author of more than 50 scientific publications devoted to the synthesis of nanocrystals and the functionalization of their surfaces for the development of next-generation photocatalysts as well as novel drug nanocarriers.

Adam Pron obtained his MSc in Chemistry and Chemical Engineering from AGH University of Science and Technology in 1974 and completed his PhD at the University of Pennsylvania (UP) in 1980 under the supervision of Alan G. MacDiarmid, 2000 Nobel Laureate in Chemistry. Then he joined the Warsaw University of Technology (WUT), becoming full professor in 1994. In 1998 he moved to the Atomic and Alternative Energies Commission (CEA) in Grenoble, France, where he initiated research on inorganic semiconductor nanocrystals. In 2012, he retired from the CEA and accepted a full-time professorship at the Warsaw University of Technology. His present research focuses on organic electroactive materials and hybrid organic–inorganic nanomaterials, including nanocrystal functionalization. He has authored over 350 scientific publications.

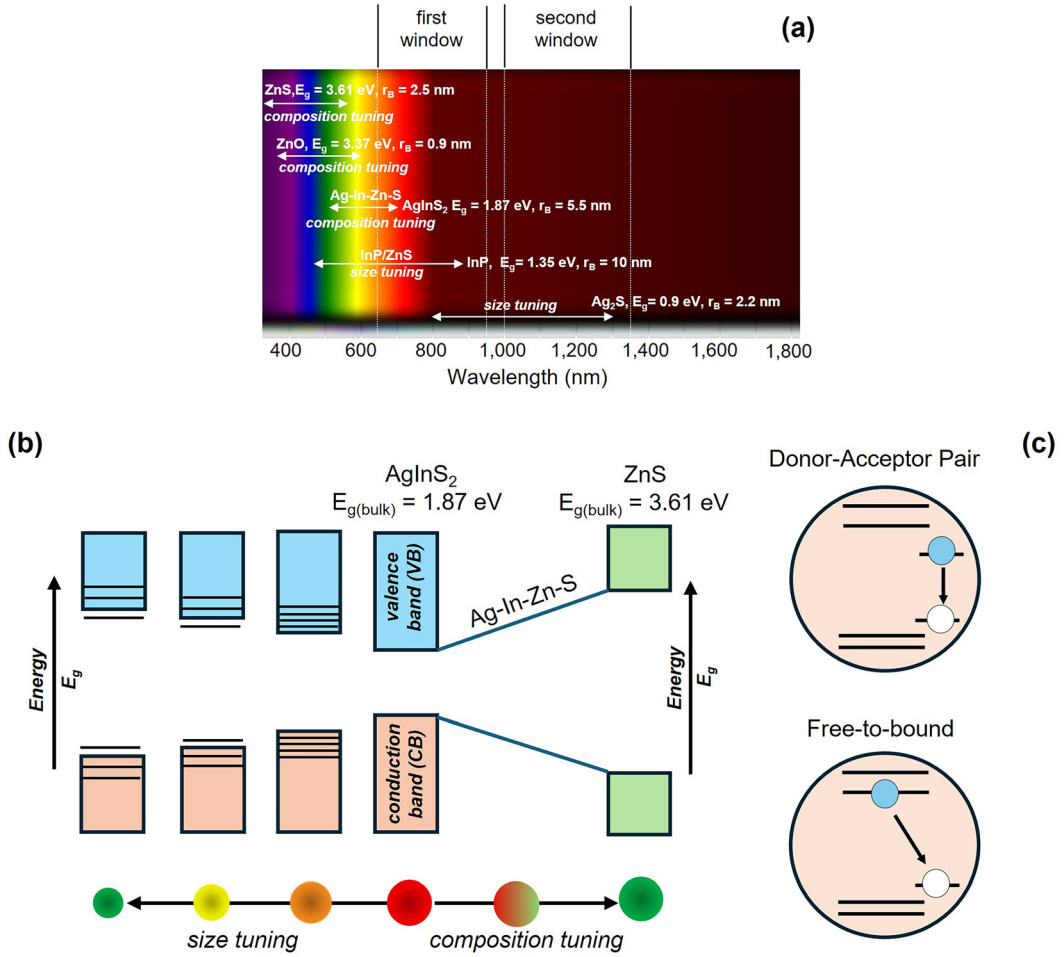

Fig. 1 (a) Luminescence range of selected QDs. (b) Schematic diagrams of the energy band gap engineering by two strategies: (i) QD size tuning and (ii) composition changes. (c) Schemes of the recombination pathways: donor–acceptor pair (mechanism: recombination of a localized electron with a localized hole) and free-to-bound (mechanism: recombination of a delocalized electron with a localized hole).

gap ($E_{g(bulk)}$) of a given semiconductor and on the value of its exciton Bohr radius (r_B), as E_g increases relative to $E_{g(bulk)}$ for nanocrystals smaller than r_B. In practice, an $E_{g(bulk)}$ in the range 2 eV to 1 eV allows for the preparation of QDs emitting light in the NIR-I range, while a gap significantly smaller than 1 eV leads to QDs emitting light in the NIR-II range. By exploiting the quantum confinement effect additional tuning of this emission in the NIR-I or NIR-II spectral range is possible. In this case, the lowest possible $E_{g(bulk)}$ value and a relatively large r_B value are advantageous, facilitating precise size control of the prepared nanocrystals. For example, in the case of the CdSe semiconductor, widely studied due to its excellent optical properties, $E_{g(bulk)}$ is equal to 1.74 eV and r_B to 5.6 nm. These values allow for the emission color tuning of CdSe nanocrystals practically over the whole visible spectral range, reaching the higher energetic part of NIR-I.[25] It is interesting to note that $AgInS_2$, a semiconductor which does not contain toxic cadmium, exhibits very similar parameters ($E_{g(bulk)}$ = 1.87 eV, r_B = 5.5 nm) to those determined for CdSe, and in consequence its nanocrystals exhibit similar optical properties.[26,27] In the case of InP, the values of $E_{g(bulk)}$ (1.35 eV) as well as r_B (10 nm) are more advantageous. Thus by exploiting the quantum confinement effect it is possible to synthesize nanocrystals emitting up to 900 nm.[28] The spectral range of NIR-II can be reached for Ag_2S nanocrystals since its $E_{g(bulk)}$ is equal 0.9–1.1 eV. The possibility of their emission tuning is, however, limited due to a rather low r_B value experimentally determined for this semiconductor (r_B = 2.2 nm).[29] Ag_2Se ($E_{g(bulk)}$ = 0.15 eV and r_B = 2.9 nm) nanocrystals can be considered as an alternative to Ag_2S ones in terms of their emission in the spectral range of NIR-II.[30,31] It should be noted that many "as prepared" nanocrystals are frequently characterized by very low photoluminescence quantum yield (PLQY). This is due to the presence of defects on their surfaces that quench luminescence. These defects can be removed by depositing an appropriate shell on the nanocrystal core, thus obtaining nanocrystals of core/shell-type.

In the case of InP nanocrystals, depositing a ZnS shell results in an increase of PLQY from <1% for InP to 60–70% for InP/ZnS.[32,33] Moreover, for core/double-shell InP/GaP/ZnS

nanocrystals PLQY values reaching 85% were reported.[34] In all these cases the shell does not affect the photoluminescence color, which is governed solely by the size of the core. As already mentioned, the value of E_g can be controllably tuned not only by exploiting the quantum confinement effect. A more practical method is the preparation of alloyed nanocrystals from semiconductors of different $E_{g(bulk)}$ values. By changing the composition of these nanocrystals, it is possible to control their E_g, which in turn allows for tuning their absorption and emission spectra. The conditions for obtaining alloyed nanocrystals are: (i) similarity of the crystal structure of the semiconductors being alloyed and (ii) a sufficiently small lattice mismatch. An instructive example worth mentioning here is the alloyed $AgInS_2$–ZnS nanocrystals, for which the $E_{g(bulk)}$ values are 1.87 eV ($AgInS_2$) and 3.61 eV (ZnS) (see Fig. 1b). Several methods of preparation of alloyed $(AgInS_2)_x(ZnS)_y$ QDs were reported[35] as well as nonstoichiometric Ag–In–Zn–S nanocrystals (*i.e.* deviating from the stoichiometry imposed by alloying) which significantly increase the range of possible compositional variations.[36,37] These QDs are characterized by high PLQY values which can be reached without the necessity of depositing of a passivation layer. They are also characterized by a large Stokes shift, a large emission peak half-width (full width at half-maximum, FWHM), and long photoluminescence lifetimes (~1.0 μs), which indicates a different radiative recombination mechanism compared to those proposed for CdSe QDs. Based on these experimental findings, new radiative recombination mechanisms were proposed, such as electron–hole recombination between localized donor and acceptor states[38–41] or, more recently, the "free to bound" mechanism involving recombination of a delocalized electron with a localized hole (see Fig. 1c).[42]

In biomedical sciences, most QD applications involve bioimaging, and utilize controlled emission from both biological windows (NIR-I and NIR-II).[43–48] On the other hand, colloidal QDs exhibit a number of other interesting properties that make them promising platforms (carriers) for controlled drug delivery.[25,49] Individual colloidal QDs are among the smallest nanoobjects, often ranging in size from 1 to 10 nm. As a consequence they are characterized by an increased fraction of surface ions (atoms) facilitating their surface functionalization. It should be emphasized here that even "as-prepared" QDs are surface-functionalized, typically with organic ligands that ensure their colloidal stability. These so-called "primary ligands", often hydrophobic in nature, for biomedical research must be exchanged for hydrophilic ones ensuring the colloidal stability of QDs in aqueous media.

More generally, through appropriate ligand exchange, it is possible to obtain not only aqueous colloidal dispersions of QDs but also dispersions in essentially all common solvents. If the ligands possess reactive end groups, the QDs can be further functionalized by attaching various types of molecule and macromolecule.[50,51] In some cases such functionalization may lead to a significant increase of the initial nanocrystals' size up to 200–500 nm. However, even then, they still retain their specific properties which can be exploited in various therapies including cancer ones.[52] For the use in bioimaging, but also in various therapies, in addition to hydrophilic ligands, bioactive moieties such as molecules of folic acid are attached to the surface of nanocrystals. Unlike normal cells, cancer cell membranes are characterized by an overexpression of folic acid receptors.[53,54] This feature is exploited in anticancer therapies.[55] Fig. 2 shows the structures of folic acid and drugs tested in QD-based hybrid drug carriers.

2. Synthesis of colloidal QDs

For the fabrication of hybrid drug nanocarriers either hydrophilic or hydrophobic QDs can be used (Table 1). In the latter case it is not always necessary to perform the ligand exchange; however the nanocrystals have to be encapsulated within a polymer shell. Alternatively, primary hydrophobic ligands can be exchanged for hydrophilic ones. This is a delicate process since it frequently results in a drastic decrease of the nanocrystal PLQY. Thus special procedures have to be elaborated capable of minimizing this undesirable effect. The third option is to introduce hydrophilic moieties from the reaction mixture as primary ligands.

2.1. Synthesis of colloidal binary QDs

Taking into account the energy gap and the exciton Bohr radius, semiconductors such as ZnO ($E_{g(bulk)}$ = 3.37 eV, r_B = 0.9 nm)[56] or ZnS ($E_{g(bulk)}$ = 3.61 eV, r_B = 2.5 nm)[57,58] cannot yield nanocrystals emitting radiation in the NIR-I let alone in NIR-II spectral ranges. It should be noted that in both cases small values of r_B severely limit the possibility of using the quantum confinement effect for tuning their absorption and emission. However, the non-toxicity of zinc and the frequent use of ZnS as a shell in QDs of a core/shell structure are arguments allowing the recognition of nanocrystals of these semiconductors as potential nanocarriers. Frequently, modification of the QDs' composition through appropriate doping is used to shift absorption and emission in the desired direction. For example, magnesium-doped ZnO nanocrystals were prepared from a mixture of $Zn(OAc)_2$/$Mg(OAc)_2$ (10/1 molar ratio) dissolved in EtOH in a two-step procedure. Nanocrystals prepared in the first step were then modified by capping with 3-aminopropyltriethoxysilane (APTES) in the second one.[59,60] The doping was spectroscopically manifested by total quenching of the emission peak at ~340 nm and the simultaneous appearance of a new peak at *ca.* 525 nm.[61] pH-sensitive emission was reported for Mg-doped ZnO QDs of sizes ranging from 3 to 4 nm; at pH = 7.4 they emitted green light whereas at pH = 5.0 this emission was quenched.[59] Defects inducing photoluminescence of ZnO nanocrystals within the visible spectral range can also be generated without the introduction of a dopant. This is the case in ZnO QDs which do not contain an admixture of magnesium. Using $Zn(OAc)_2$ and sodium or potassium hydroxides in the presence of EtOH, it is possible to obtain amine-capped ZnO QDs in a two-step process, for which green emission is observed at approximately

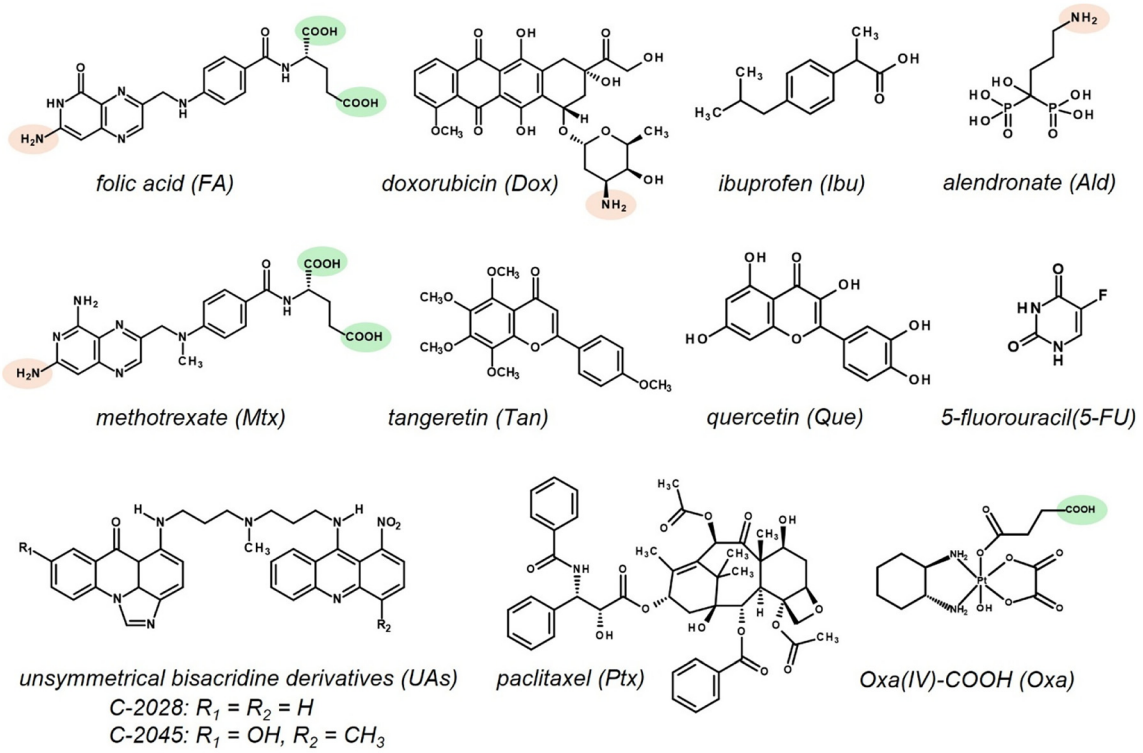

Fig. 2 Structures of folic acid and drugs tested in QD-based hybrid drug nanocarriers.

540 nm.[62,63] This broad peak present in the emission spectra of aqueous dispersions of amine-capped ZnO-NH_2 QDs is attributed to transitions associated with oxygen vacancy defects. The accompanying two peaks at 377 nm and 415 nm originate from the QDs.[63,64] ZnO nanocrystals emitting radiation in the visible range of the spectrum can also be synthesized *via* the organometallic route.[65] For example, QDs obtained from Et_2Zn-based precursors and capped with sulfoxide ligands were characterized by a size distribution of 5.4–8.2 nm and exhibited green photoluminescence of very long lifetimes.[66]

Mn^{2+} ions are often chosen as dopants for ZnS nanocrystals. For example Mn-doped ZnS quantum dots were obtained starting from a mixture of $ZnSO_4/MnCl_2$ precursors with a molar ratio of 12.5/1.0 using Na_2S as a source of sulfur. The reactions were carried out in aqueous solutions at room temperature. As-prepared QDs were then surface-modified by reaction with 3-mercaptopropyltriethosysilane (MPTS).[67] These Mn-doped ZnS QDs emitted light at a wavelength of 600 nm characterized by long decay times of *ca.* 1.3 ms. For comparison, aqueous dispersions of ZnS QDs containing no manganese (~4 nm in size) and stabilized with hydrophilic ligands (carboxymethylcellulose, CMC) were characterized by an emission peak with a maximum at approximately 426 nm.[68]

InP ($E_{g(bulk)}$ = 1.35 eV, r_B = 10 nm), due to its low $E_{g(bulk)}$ and relatively high r_B, is almost ideally suited for the preparation of nanocrystals of tunable emission covering almost the entire NIR-I range. This range is even available for small-sized nanocrystals (<5 nm).[69] As already mentioned, in the case of InP QDs it is necessary to deposit a ZnS or ZnSe passive layer on the InP core, otherwise the measured PLQY is very low (<1%). A two-step strategy is usually used in the preparation of InP/ZnS QDs for biological and biomedical applications. In the first step, QDs stabilized with hydrophobic ligands, primarily long-chain carboxylic acids, are obtained. These ligands are then exchanged for hydrophilic ones in the second step, yielding dispersions stable in aqueous media. A number of synthetic procedure methods have been developed over the last 20 years enabling strict size and shape control of InP nanocrystals.[70] In these optimization procedures the use of the non-coordinating solvent 1-octadecene (ODE) is considered crucial,[71] as well as replacing the expensive and unstable phosphorus precursor $P(TMS)_3$ – tris(trimethylsilyl)phosphine, first with gaseous PH_3 generated *in situ* due to its toxicity[72] and then with stable and non-toxic tris(diethylamino)phosphine.[73] The principal methods of the preparation of core/shell InP/ZnS nanocrystals are based on a two-step reaction with no separation of InP particles from the reaction mixture. In the first step, starting from a mixture of $In(OAc)_3$ and myristic acid (MA) in ODE, a solution of $P(TMS)_3$ in 1-octylamine is injected. The nanocrystal size is controlled by the MA concentration and the reaction conditions (temperature and time). In the second step, a ZnS layer is deposited by alternate injections of zinc stearate $Zn(SA)_2$ and sulfur solutions, both dissolved in ODE. This method was used in the preparation of a series of InP/ZnS nanocrystals emitting light in the range of 450 to

Table 1 Synthesis conditions for hydrophilic QDs used as components of drug nanocarriers

QDs	Precursors, ligands, solvent and reaction conditions	Size (nm)	Photoluminescence, λ_{em} (nm)/PLQY (%)	Ref.
ZnO-Mg	1. $Zn(OAc)_2/Mg(OAc)_2$ = 10.0/1.0, EtOH + NaOH/EtOH, r.t., 8 h 2. APTES, DMF, 120 °C, 15 min	3–4	525/—	59 and 60
ZnO	1. $Zn(OAc)_2$/EtOH + KOH/EtOH, r.t., 1 h 2. APTES/EtOH + water, r.t. 2 h	~3	525/—	62
ZnO	1. $Zn(OAc)_2$/EtOH + NaOH/EtOH, reflux, 20 min 2. APTES/NMP, 120 °C, 20 min	4–5	377, (415), 536/—	63
ZnS-Mn	1. $ZnSO_4/MnCl_2$ = 12.5/1.0, water + Na_2S/water, r.t., 30 min 2. MPTS/EtOH, r.t., 20 h	~12	600/~15	67
ZnS	$ZnCl_2$, CMC, water (pH = 7.5) + Na_2S/water, r.t., 30 min	~4	426/—	68
InP/ZnS	1. $In(OAc)_3$/MA = 1/3, ODE + PH_3 (Ca_3P_2 + HCl), 250 °C, 1 h 2. $Zn(SA)_2$/ODE, zinc ethylxanthate/ODE, 210 °C, 30 min 3. Cys, TGA, 3-MPA, DHLA, MUA, pH (9–12)	5–6	>700/4–42	69 and 72
Ag_2S	$(C_2H_5)_2NCS_2Ag$, OA, ODA, ODE, 200 °C, 30 min	~10	1058/—	76
Ag_2S	AgOAc, MA, 1-octylamine, ODE + $(TMS)_2S$/TOP, 50–120 °C	1.5–4.6	690–1227/~13	77
Ag_2S	1. $(C_2H_5)_2NCS_2Ag$, DDT, 210–230 °C, 1 h 2. DHLA/EtOH, r.t., 48 h	~5	1200/6	78
Ag_2S	$AgNO_3$, 2-MPA, water (pH = 7.5) + Na_2S/water, 30–90 °C, 1–3 h	2.2–3.1	780–950/7–39	79
Ag_2S	$AgNO_3$, GSH, water (pH = 4,5,7 or 10) + Na_2S/water, r.t.–50 °C	2–4	700–900/14	80
Ag_2S	$AgNO_3$, MPEG-SH/HOOCPEGSH, water (pH = 3 or 7.5) + Na_2S/water, 90 °C, 90–120 min	2–3	775–930/2–66	81
Ag_2Se	AgTFA + $Li[N(Si(CH_3)_3)_2]$/OLA + Se/TOP, 70 °C, 1 h	2.0 (3.5)	1030(1250)/2	83
Ag_2Se	$AgNO_3$ + Ala (NaOH, pH = 13) 90 °C + Na_2SeO_3, GSH, NADPH, GR (pH = 7.1), 90 °C, 10 min	1.5 (2.4)	700(820)/1(3)	86
Ag_2Se	1. $AgNO_3$-OLA/toluene + NaHSe/DDT, autoclave, 180 °C, 1 h 2. C18-PMH-PEG/chloroform, r.t., 12 h,	3.4	1300/—	85
Ag_2Se	1. AgOAc, 1-octanethiol, ODE + Se/TOP, 130 °C, 1 h 2. MUA/EtOH, 12 h	3.9	1180/3	84
$AgInSe_2$/ZnS	1. $AgNO_3$, $In(OAc)_3$, ODE, DDT, OA + Se/OLA + DDT, 175 °C, 30 min 2. + S + $Zn(SA)_2$/OLA + ODE, 175 °C, 90 min 3. QDs/chloroform + octylamine modified PAA/water, shaken, 10 min	6.5	820/40	93
$AgInS_2$	$AgNO_3$, $In(NO_3)_3$, GSH, water (pH = 8.5) + Na_2S, 100 °C, 2 h	6.1	634/21	96
$AgInS_2$/ZnS	1. $AgNO_3$, $In(SA)_3$, OA, DDT, ODE + S/ODE, 150 °C 2. + $Zn(SA)_2$/ODE, zinc ethylxanthate/DMF, 180 °C 3. + PMO/chloroform	3.5	520/60	97
Ag–In–Zn–S	1. $AgNO_3$, $InCl_3$, $Zn(SA)_2$, DDT, ODE + S/OLA, 180 °C, 1 h 2. +MUA/NaOH, water, 80 °C, 8 h	5.6	730/30	36 and 100

r.t. – room temperature, Ala – L-Alanine, AgTFA – silver trifluoroacetate, APTES – 3-aminopropyltriethoxysilane, MPTS – 3-mercaptopropyltriethoxysilane, CMC – carboxymethylcellulose (M_w = 250 kDa), DDT – 1-dodecanethiol, DMF – *N*,*N*′-dimethylformamide, NMP – *N*-methylpyrrolidone, ODE – 1-octadecene, OLA – oleylamine, OA – oleic acid, ODA – *n*-octadecylamine, MA – myristic acid, $Zn(SA)_2$ – zinc stearate, Cys – cysteine, TGA – thioglycolic acid, TOP – trioctylphosphine, DHLA – dihydrolipoic acid, 2-MPA – 2-mercaptopropionic acid, 3-MPA – 3-mercaptopropionic acid, MUA – 11-mercaptoundecanoic acid, GSH – 2-glutathione (tripeptide: γ-Glu–Cys–Gly), GR – yeast glutathione reductase, NADPH – nicotinamide adenine dinucleotide phosphate, C18-PMH-PEG – amphiphilic poly(maleic anhydride-*alt*-1-octadecene)-methoxy poly(ethylene glycol), PAA – poly(acrylic acid) (M_w = 3000 Da), PMO – poly(maleic anhydride-*alt*-1-octadecene) (M_w = 3000–5000).

750 nm with a PLQY of ~40%. Moreover, the exchange of primary hydrophobic ligands for hydrophilic 3-mercaptopropionic acid (3-MPA), carried out at pH = 10, did not worsen their luminescence properties.[74] In a different two-step procedure, InP/ZnS QDs exhibiting tunable emission in the spectral range of 675–720 nm were synthesized. In the first step, InP nanocrystals were obtained by introducing PH_3 (generated in the reaction of Ca_3P_2 with HCl) into a mixture of $In(OAc)_3$/MA = 1/3 dissolved in ODE, while ZnS was introduced by sequential addition of $Zn(SA)_2$ and zinc ethylxanthate dissolved in ODE.[72] For this series of nanocrystals, procedures of exchanging the primary hydrophobic ligands (stearic acid, SA) for hydrophilic ones such as cysteine (Cys), thioglycolic acid (TGA), dihydrolipoic acid (DHLA), 11-mercaptoundecanoic acid (MUA) and 3-MPA were elaborated. The obtained stable aqueous dispersions emitted red light (λ_{max} at *ca.* 700 nm).[69]

As already mentioned, for Ag_2S $E_{g(bulk)}$ values range from 0.9 to 1.1 eV, depending on the crystal structure of a given polymorph. For Ag_2Se, $E_{g(bulk)}$ is equal to 0.15 eV. Low values of this parameter clearly indicate that it is viable to prepare Ag_2S and Ag_2Se QDs emitting radiation in both the NIR-I and NIR-II spectral ranges. Furthermore, both semiconductors are characterized by ultralow solubility; their solubility products are 6.3×10^{-50} and 2.0×10^{-64} for Ag_2S and Ag_2Se, respectively. This limits the concentration of free silver ions released into the solution and facilitates the formation of their colloidal nanocrystals.[75] For both semiconductors, precise tuning of their spectroscopic properties is typically achieved either by exploiting the quantum confinement effect or by modifying their composition, or even by combining these two effects. Due to the high interest in the applications of Ag_2S and Ag_2Se nanocrystals, a number of preparation methods have been

developed in recent years yielding QDs of these semiconductors stabilized by hydrophobic or hydrophilic ligands.

One of the first methods for obtaining Ag_2S QDs involved the decomposition of the complex precursor $(C_2H_5)_2NCS_2Ag$ in a mixture of oleic acid (OA) and *n*-octadecylamine (ODA) ligands dissolved in ODE. The resulting Ag_2S QDs 10.2 ± 0.4 nm in size emitted NIR radiation (λ_{max} = 1058 nm).[76] By precisely varying the size of the QDs from 1.5 to 4.6 nm, Pang *et al.* achieved strict control of their emission in the 690 to 1227 nm range.[77] The reactions were carried out using the hot-injection method, introducing a solution of $(TMS)_2S$ – hexamethyldisilathiane in TOP (trioctylphosphine) into a mixture of silver acetate, MA, and 1-octylamine dissolved in ODE.

The size of the formed nanocrystals was controlled by carrying out the reaction at different temperatures and varying its time. Additionally, a method for exchanging hydrophobic primary ligands for hydrophilic ones (MUA) was developed, resulting in stable aqueous dispersions of Ag_2S nanocrystals.[77]

More recently, a series of size-controlled Ag_2S QDs, covering the range from 2.4 to 7.0 nm, was synthesized. These studies allowed for precise tuning of the emission in the spectral range from 975 to 1175 nm as well as for the determination of the exciton Bohr radius, r_B = 2.2 nm. The heating-up method was applied consisting of decomposing the complex precursor $(C_2H_5)_2NCS_2Ag$ dissolved in 1-dodecanethiol (DDT) which served as both ligand and solvent. Size control was achieved by conducting the decomposition reaction at different temperatures and times.[29] QDs prepared in this manner could be rendered hydrophilic by exchanging primary DDT ligands for hydrophilic DHLA. The resulting aqueous dispersions were colloidally stable and emitted light in the NIR-II spectral range (λ_{max} = 1200 nm).[78]

A preparative method was also developed to directly obtain Ag_2S QDs stabilized with hydrophilic primary ligands. The reaction was carried out in water at pH = 7.5 using $AgNO_3$ and Na_2S as silver and sulfur precursors together with 2-mercaptopropionic acid (2-MPA) as the ligand.[79] The same precursors were used in another method, which however employed a different and more complex hydrophilic ligand, namely glutathione (GSH) – a tripeptide: γ-Glu–Cys–Gly. The reactions were carried out at different pH values (4.5, 7.0, or 10.0) and at temperatures ranging from room temperature to 50 °C, which allowed for the control of the Ag_2S QDs emission in the range of 700 to 900 nm.[80] In yet another version of this reaction, hydrophilic polymers such as polyethylene glycols containing an –SH end group (MPEG-SH, M_w = 2000 or 5000) and polyglycols with –SH and –COOH end groups (CMPEG-SH, M_w = 2000) were used as ligands. The reactions were carried out in the presence of differently composed mixtures of ligands and at different pH values. The resulting aqueous dispersions of Ag_2S QDs differing in size emitted radiation in the spectral range from 775 to 930 nm, with a high PLQY exceeding 60%.[81] O. El-Dahshan *et al.* synthesized hydrophilic Ag_2S QDs *via* a combined hydrothermal (140 °C) and microwave-assisted approach.[82] The reaction was performed in an aqueous solution containing silver nitrate and glutathione (GSH), with ammonium hydroxide added to adjust the pH to 8.0. By changing the $AgNO_3$/GSH molar ratio and reaction time, Ag_2S quantum dots with diameters of approximately 4–17 nm were obtained, exhibiting emission in the 950–1220 nm range. MTT assays confirmed their biocompatibility toward HepG2/C3A cells. Based on these studies, it was concluded that an increase in crystallite size and crystallinity of the quantum dots resulted in reduced toxicity of these QDs.[82]

Ag_2Se is a semiconductor characterized by a very low $E_{g(bulk)}$ value, which additionally significantly differs depending on the structure of a given polymorph. For orthorhombic Ag_2Se, $E_{g(bulk)}$ = 0.15–0.18 eV, while for the tetragonal one, $E_{g(bulk)}$ = 0.07 eV with r_B = 2.9 nm.[31] One of the first procedures of the preparation of Ag_2Se quantum dots involved the metathesis reaction between silver trifluorooctane (AgTFA) and lithium silylamide, resulting in the formation of silver silylamide (Ag$[N(Si(CH_3)_3)_2]$). To this silver complex dissolved in oleylamine (OLA), solution of selenium in TOP was then added. Orthorhombic Ag_2Se QDs of size 2.0 and 3.4 nm were obtained, characterized by NIR-II photoluminescence at 1030 and 1250 nm, respectively.[83] Orthorhombic Ag_2Se QDs were also synthesized using the hot-injection method. In this procedure, a selenium precursor (Se/TOP) was injected into a mixture of AgOAc and 1-octanethiol dissolved in ODE. In the next step the primary hydrophobic ligands were exchanged for hydrophilic ones (MUA), yielding stable aqueous dispersions of Ag_2Se nanocrystals (3.9 nm in size) which emitted radiation at *ca.* 1200 nm.[84]

Dong *et al.* proposed an interesting method for hydrophilization of hydrophobic QDs which was different from the "classical" ligands exchange.[85] According to their procedure, orthorhombic Ag_2Se QDs with a size of 3.4 nm were transferred to the aqueous phase without exchanging the hydrophobic primary ligands but by exploiting the phenomenon of their encapsulation with an amphiphilic alternating copolymer, namely poly(maleic anhydride-*alt*-1-octadecene)-methoxy poly (ethylene glycol) (C18-PMH-PEG). Aqueous dispersions of these nanocrystals emitted radiation in the NIR-II spectral range (λ_{max} = 1300 nm).[85] Direct methods for preparing hydrophilic quantum dots are interesting because they allow avoiding the ligand exchange step. One such method for obtaining orthorhombic Ag_2Se quantum dots was proposed by Gu *et al.*[86] According to this procedure, the silver precursor *i.e.* alanine complex of Ag^+(Ag^+-Ala) was mixed with a selenium precursor obtained through reduction of Na_2SeO_3 in the presence of a hydrophilic ligand (GSH), nicotinamide adenine dinucleotide phosphate (NADPH) and yeast glutathione reductase (GR). Two Ag : Se ratios were tested, namely 6 : 1 and 4 : 1, yielding nanocrystals of 1.4 nm and 2.4 nm, respectively. These QDs emitted radiation within the NIR-I spectral range (700 nm and 820 nm).[86]

2.2. Synthesis of colloidal ternary QDs

The preparation methods described above concerned QDs of binary semiconductors. Research on ternary semiconductor nanocrystals began later, but has been attracting growing inter-

est for the past 15 years. Silver indium chalcogenides, such as $AgInSe_2$ ($E_{g(bulk)}$ = 1.24 eV) and $AgInS_2$ ($E_{g(bulk)}$ = 1.87 eV), are particularly noteworthy in this respect, not only for their spectroscopic properties but also for their high biocompatibility and natural circulation in the environment.[87] These properties make them advantageous over ternary chalcogenides containing copper ($CuInSe_2$ ($E_{g(bulk)}$ = 1.05 eV) and $CuInS_2$ ($E_{g(bulk)}$ = 1.53 eV)), whose biocompatibility and toxicity is a matter of debate.[88]

The synthesis of ternary semiconductor nanocrystals is generally a more challenging task than the preparation of binary nanocrystals. The main difficulty lies in selecting precursors of both metals so that their balanced reactivity toward the sulfur (selenium) precursor leads to a single-phase ternary product, rather than a mixture of different phases. However, varying the precursor's reactivity is necessary when the goal of research is to vary the composition of ternary QDs either through alloying or by preparation of truly non-stoichiometric nanocrystals. Controlling the composition allows, in turn, for tuning the nanocrystal absorption and emission and also affects their PLQY. In many cases, achieving a high PLQY value requires the deposition of an appropriate passivating shell or the preparation of quaternary nanocrystals either by alloying with ZnS (or ZnSe) or by fabricating truly nonstoichiometric quaternary nanocrystals of the following type: Ag(Cu)–In–Zn–S(Se). In the latter case high values of PLQY can be reached without the necessity of depositing a passivating shell.[89,90] Historically, the first method for obtaining ternary Ag–In–S nanocrystals was proposed by P. M. Allen and M. G. Bawendi.[91] Starting from a mixture of AgI and InI_3, OLA, and TOP, into which a selenium precursor in the form of a solution of $((CH_3)_3Si)_2Se$ in TOP was injected, QDs of the composition $Ag_{1.00}In_{1.33}Se_{2.57}$ were obtained. These nanocrystals were characterized by emission at approximately 600 nm with PLQY = 15%. Yarema *et al.* developed a preparative procedure for obtaining QDs of varying sizes and compositions.[92] In this method, a mixture of selenium dissolved in TOP and $LiN(Si(CH_3)_3)_2$ was injected into a mixture of AgI and InI_3 in TOP. Nanocrystals of controlled size were obtained covering the range from 2.4 to 7 nm. Their composition could also be varied from QDs strongly enriched in indium ($AgIn_{11}Se_{17}$) to stoichiometric ones ($AgInSe_2$). The synthesized nanocrystals emitted radiation in the range of 600 to 1100 nm. For QDs of the composition $Ag_3In_5Se_9$, the measured PLQY was 21%, while after depositing a ZnSe layer, the PLQY increased to 73%.

In the method proposed by Deng *et al.* Se dissolved in a mixture of OLA and DDT was injected into a mixture consisting of $AgNO_3$, $In(OAc)_3$, DDT and OA dissolved in ODE.[93] The Ag : In molar ratio was varied from 0.4 : 1.2 to 1.0 : 1.0. The resulting QDs exhibited emission in the range from 700 to 820 nm, albeit with low PLQY. After deposition of a ZnS layer on the $AgInSe_2$ core, the PLQY value increased to 40%. The resulting $AgInSe_2$/ZnS nanocrystals could be transferred to the aqueous phase without the necessity of exchanging hydrophobic ligands, simply by encapsulation with an amphiphilic polymer, namely octylamine-modified poly(acrylic acid). A direct method for the large-scale synthesis of hydrophilic $AgInSe_2$/ZnS QDs was also reported.[94] In this procedure the synthesis was carried out in a 5 L electric pressure cooker under gentle heating. In the first step, $AgInSe_2$ QDs were prepared from a mixture consisting of $AgNO_3$, $In(OH)_3$, TGA, $NH_3{\cdot}H_2O$ and a selenium precursor obtained by dissolving Se in $NaBH_4$ and water in the presence of gelatin. After an hour of reaction, a zinc precursor prepared by dissolving ZnO in an aqueous solution of ammonium thioglycolate and a sulfur precursor, namely thiourea dissolved in water, were added to the reaction mixture, and the reaction was continued under the same conditions. The obtained $AgInSe_2$/ZnS QDs were characterized by emission in the range of 582 to 686 nm, reaching a maximum PLQY of 23%.[94]

The crystal structure of ternary Ag–In–S nanocrystals is strictly dependent on their composition. In the case of QDs of stoichiometric ($AgInS_2$) or near stoichiometric compositions, either orthorhombic or tetragonal nanocrystals can be obtained. Nanocrystals characterized by a significant indium excess, such as $AgIn_5S_8$, adopt a cubic structure. Varying the structure type and composition of non-stoichiometric Ag–In–S nanoparticles translates into the possibility of tuning their absorption and emission ranges and, in some cases, also PLQY values. In this context, it is worth mentioning the study presenting the possibility of obtaining stoichiometric and non-stoichiometric ternary Ag–In–S nanocrystals by thermal decomposition of a single complex precursor, which is the source of all three elements constituting the ternary QDs, namely $Ag_xIn_{(1-x)}[S_2CN(C_2H_5)_2]_{(3-2x)}$. By changing x in the precursor, it is possible to change the composition of the obtained nanocrystals.[95] A series of these one-component complex precursors, with N_{Ag}/N_{metal} molar ratios varying from 0.1 to 0.7, were decomposed at 180 °C in the presence of primary amines, namely oleylamine (OLA) or *n*-octylamine. Increasing N_{Ag}/N_{metal} gave rise to a linear increase of the silver content in the resulting QDs and, at the same time, allowed for precise emission tuning in the range from 650 to 830 nm. Significant changes in the QD crystal structure could be noted, from the cubic characteristic of $AgIn_5S_8$ for low silver content (0.1) through orthorhombic to tetragonal for the highest silver content (0.7). Clear differences in PLQY were also observed; in the case of N_{Ag}/N_{metal} = 0.37, the highest PLQY equal to 70% was measured.[95] Diversification of the composition of nanocrystals obtained from a single complex precursor is often difficult and requires complicated syntheses. An alternative is the use of a mixture of simple precursors, especially useful in the preparation of colloidal non-stoichiometric Ag–In–S QDs. In some cases this approach allows for the direct introduction of hydrophilic capping ligands. This approach was used by M. Hashemkhani *et al.* who prepared nonstoichiometric ternary nanocrystals from a mixture of $AgNO_3$, $In(NO_3)_3$, and GSH dissolved in water at pH = 8.5, to which a Na_2S solution was added.[96] Then the whole mixture was heated at 100 °C. Starting from a mixture of precursors with a molar ratio of Ag/In = 1/4, nanocrystals with the composition $Ag_{1.0}In_{3.5}S_{2.0}$ were obtained, characterized by emission at 634 nm and a PLQY =

21%. The multiprecursor approach was also adapted for the preparation of core/shell $AgInS_2$/ZnS and nonstoichiometric quaternary Ag–In–Zn–S QDs. In one of the proposed strategies, the first preparation step involved the introduction of a sulfur precursor (S/ODE) to a mixture of $AgNO_3$, $In(SA)_3$, OA, and DDT in ODE to yield $AgInS_2$. In the second step, the ZnS shell was deposited through injection of $Zn(SA)_2$/ODE and zinc ethylxanthate/DMF. Subsequently, the obtained QDs were encapsulated using PMO (poly(maleic anhydride-*alt*-1-octadecene)), which allowed for their transfer to aqueous media. The resulting $AgInS_2$/ZnS QDs were characterized by emission at 520 nm and a PLQY value of 60%.[97]

A number of preparative procedures developed in the last decade allowed for the synthesis of non-stoichiometric quaternary Ag–In–Zn–S QDs with controlled composition, tunable emission, and high PLQY without the necessity of depositing a passivating shell. In a typical preparation, a sulfur precursor in the form of S/OLA was injected into a mixture of metal precursors ($AgNO_3$, $InCl_3$, $Zn(SA)_2$, and DDT) in ODE as a solvent, with varying molar ratios. A series of nanocrystals with different compositions were obtained, exhibiting emission in the range of 552 to 730 nm.[36] Optimization of this procedure led to the preparation of non-stoichiometric nanocrystals of compositions $Ag_{1.00}In_{1.50}Zn_{7.80}S_{17.0}$ and $Ag_{1.00}In_{2.80}Zn_{1.30}S_{4.00}$, characterized by green (543 nm) and red (720 nm) light emission with PLQY values of 48% and 67%, respectively.[98,99] For these nanocrystals, effective methods of exchanging hydrophobic ligands for hydrophilic ones such as MUA, DHLA, and Cys, were developed while preserving their excellent photoluminescence properties.[100] An interesting method for the synthesis of nonstoichiometric quaternary Ag–In–Zn–S QDs was also developed in recent years. In this procedure, In(II) in the form of the In_2Cl_4 dimer was used for the first time as a source of indium, together with the remaining metal precursors, namely $AgNO_3$ and $Zn(SA)_2$ as well as DDT, all dissolved in ODE. The sulfur precursor (S/OLA) was then injected into this mixture. By controlling the molar ratios of the metal precursors, the composition of the resulting Ag–In–Zn–S QDs could be varied, yielding nanocrystals of tunable photoluminescence covering the spectral range from *ca.* 530 to 730 nm.[37] A new method of exchanging hydrophobic ligands for hydrophilic ones (MUA) was also developed for quaternary Ag–In–Zn–S QDs in which ultrasonic assistance was applied for the first time. This procedure proved to be not only more efficient but also allowed the exchange to be carried out under significantly milder conditions. The QDs obtained in this way, with compositions of $Ag_{1.0}In_{2.7}Zn_{30.0}S_{90.0}$ and $Ag_{1.0}In_{1.3}Zn_{0.5}S_{3.3}$, exhibited emission at 545 and 795 nm, respectively, with a PLQY of 15% and 20%.[101] Finally, it is worth mentioning the hydrophilic Ag–In–Zn–S QDs obtained by direct synthesis in which primary ligands were hydrophilic in nature and no ligand exchange was necessary. In this case, aqueous Na_2S solution was added to a mixture of $AgNO_3$, $In(NO_3)_3$, and 3-MPA in water at pH = 8.5. The resulting Ag–In–S QDs in the form of an aqueous dispersion were then treated with a zinc precursor ($Zn(OAc)_2$) and the whole mixture was heated at 90 °C for 90 minutes. By changing the molar ratio of the precursors, Ag–In–Zn–S QDs of different compositions were obtained, characterized by emission in the spectral range of 540 to 610 nm, with a maximum PLQY reaching 78%.[102]

For the same family of quaternary QDs (Ag–In–Zn–S), a strategy for coating the nanocrystal surface with a SiO_2 shell was also reported.[103] Using QDs capped with hydrophobic primary ligands, cetyltrimethylammonium bromide was introduced in the first step to enable phase transfer and surface modification. Subsequently, the SiO_2 shell was grown in the presence of an aqueous solution containing sodium hydroxide and tetraethyl orthosilicate (TEOS). This approach allowed precise control over the silica shell thickness within the 10–20 nm range, while keeping the overall particle diameter below 50 nm. The resulting aqueous dispersions of Ag–In–Zn–S@SiO_2 QDs displayed stable photoluminescence over time, with an emission maximum located at approximately 700 nm.[103]

3. Synthesis of colloidal carbon dots

Numerous similarities can be observed between inorganic semiconductor quantum dots (QDs) and carbon dots (CDs). The sizes of synthesized CDs typically fall within a similar diameter range of 1–10 nm, in which quantum confinement effects are clearly observed. By controlling the size of the CDs and the nature of the generated surface defects, it is possible to tune their absorption and emission spectra across the 300–800 nm wavelength range.[104,105]

CDs were first isolated in 2004 by means of preparative electrophoresis during the purification of single-walled carbon nanotubes derived from arc-discharge soot.[106] However, Sun *et al.*[107] first obtained CDs in 2006 by chemical synthesis using laser ablation of a carbon target in the presence of water vapor with argon as the carrier gas. The as-obtained, non-functionalized CDs did not exhibit photoluminescence and therefore required surface passivation to impart emissive properties. This process involved the attachment of selected organic species to the surface of acid-treated CDs. Surface passivation with diamine-terminated oligomeric poly(ethylene glycol), $(H_2NCH_2(CH_2CH_2O)_nCH_2CH_2CH_2NH_2$; average n ~35; PEG1500N), yielded CDs exhibiting emission in the range of *ca.* 400 to *ca.* 690 nm, with the PLQY in the range of 4–10%. The pronounced variation in emission colour was attributed to the quantum confinement effect arising from differences in the CDs' size.[107]

Jiang *et al.*[108] used *o*-phenylenediamine, *m*-phenylenediamine, and *p*-phenylenediamine as surface passivating agents in the solvothermal synthesis of CDs carried out at 180 °C, yielding nanoparticles with average diameters of 6.0, 8.2, and 10.0 nm, respectively. For these CD dispersions, a pronounced bathochromic shift of the emission band was observed with increasing particle size, from 435 nm for the smallest CDs, through 535 nm for the intermediate ones, to 604 nm for the largest particles, under excitation at 365 nm. A

distinct feature of the studied nanoparticles was the excitation-wavelength dependence of both the emission maximum and the PLQY. In the case of 10 nm CDs, the PLQY increased from 20.6% to 26.1% as the excitation wavelength changed from 365 to 510 nm. Photoluminescence decay analysis revealed PL lifetimes in the range of 1–9 ns.[108] The solvothermal method was also employed by Wang *et al.*[109] Starting from mixtures of *o*-phenylenediamine with various acids – including 4-aminobenzenesulfonic acid, folic, boric, acetic, terephthalic, and tartaric acids in ethanol – these authors synthesized a series of CDs with average diameters ranging from 1.7 to 2.4 nm.

A pronounced quantum confinement effect was observed with decreasing particle size, manifested as an increase in the bandgap energy (E_g) from 1.9 to 2.8 eV and a corresponding shift of the emission maximum from 600 to 355 nm. The measured the PLQY ranged from 25 to 72%, with PL lifetimes not exceeding 10 ns.[109]

Carbon dots (CDs) exhibit unique optical properties beyond fluorescence, as they can also display phosphorescence with lifetimes of the order of milliseconds when appropriately chemically modified. For example, CDs with an average diameter of ~5 nm, synthesized *via* pyrolysis of ethylenediaminetetraacetic acid disodium salt and dispersed in a polyvinyl alcohol (PVA) matrix, demonstrated room-temperature phosphorescence. Upon excitation with UV light (325 nm), phosphorescence was observed with a maximum at 500 nm and a long lifetime of approximately 380 ms. Studies indicated that the observed phosphorescence originates from the presence of aromatic carbonyl groups, while the PVA matrix stabilizes their triplet states, protecting them from quenching by intramolecular motions and molecular oxygen.[110] Currently developed preparative methods enable the synthesis of CDs exhibiting phosphorescence across the entire visible spectrum.[111] Examples of CDs exhibiting phosphorescence in the near-infrared (NIR) region have been reported in the literature. Geng *et al.*,[112] for instance, employed a one-step microwave-assisted strategy to synthesize NIR-phosphorescent CDs. The resulting nanoparticles were finely decorated with sulfonic (SO_3^-) acceptors and pyrrolic/graphitic nitrogen donors. Indocyanine green (ICG) and branched polyethylenimine (BPEI) were used as the precursors in this synthesis. These CDs, with an average size of approximately 2.7 nm, exhibiting a bandgap (E_g) of 1.6 eV and emitting near-infrared (NIR) radiation at 760 nm (17.6% quantum yield; 11.4 μs lifetime), were employed to construct a theranostic platform, CD@CCM. The platform utilized cancer cell membranes (CCM) as both a targeting agent and a delivery system for NIR imaging-guided sonodynamic therapy.[112]

In the synthesis of CDs, both conventional *bottom-up* approaches and *top-down* strategies are employed. Moreover, CDs can be classified as biogenic nanoparticles,[113,114] which can be obtained directly from bioorganic precursors, including silk,[115] orange juice,[116] banana juice,[117] honey,[118,119] and even food waste.[120] Similar to inorganic semiconductor quantum dots (QDs), CDs are primarily employed in biomedical applications, particularly for bioimaging,[121–123] and only to a limited extent as drug delivery carriers.

4. Types of hybrid used as nanocarriers

The presence of toxic metals in the initially synthesized QDs practically limited the possibilities of their use as nanocarrier components to those which can be encapsulated. In contrast, in the case of toxic metal-free QDs, it is possible to elaborate various nanocarrier design strategies, as evidenced by numerous examples in the literature. For the purpose of this study, we have classified these hybrids into three groups, A, B, and C, based on the role of the ligands and the type of bond(s) used for attaching the nanocarrier to the drug (Fig. 3 and Tables 2, 3). In the case of **type A hybrids**, QDs are stabilized with hydrophilic ligands, while non-covalent interactions are exploited for binding the drug to them. In **type B hybrids**, QDs are also stabilized with hydrophilic ligands but these are further functionalized by binding to them moieties which act as linkers or bioactive molecules – targeting ligands. In this case, drugs can be bound to these functionalized ligands either through non-

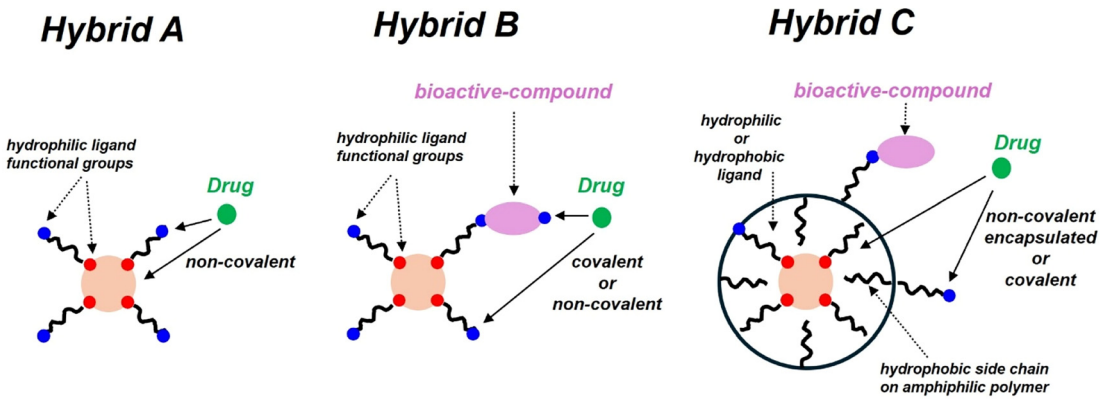

Fig. 3 Types of hybrid used as drug nanocarriers.

Table 2 **Type A** and **type B** hybrids, composition, size, λ_{em} and applications

Hybrid composition – QDs + ligands + drugs	Drug	Size(nm)/ λ_{em}(nm)	Applications	Ref.
ZnO-Dox (non-covalent)	Dox	~40[a]/em. quenching	*In vitro*, breast cancer cells (MCF-7R)	124
ZnS-CMC-Dox (non-covalent)	Dox	~58[b]/em. quenching	*In vitro*, brain cancer cells (U-87 MG)	68
ZnO-NH_2-Tan (non-covalent)	Tan	~5[a]/377, 536	*In vitro*, lung cancer cells (H538)	63
$\mathbf{Ag_{1.0}In_{1.2}Zn_{5.6}S_{9.4}}$/MUA-UAs (non-covalent)	UAs	3.1[a]/576	*In vivo*, *in vitro* lung H460 and colon HCT116 cancer cells	127
$\mathbf{Ag_{1.0}In_{1.0}Zn_{1.0}S_{3.5}}$/MUA-UAs (non-covalent)		5.8[a]/730		128
ZnO-NH_2 + HOOC-PEG-COOH (covalent) + HA (covalent) + Dox (non-covalent)	Dox	~6[a]/em. quenching	*In vitro*, lung cancer cells (A549)	131
ZnO-NH_2 + PBA (covalent) + Que (non-covalent)	Que	~400[b]/527	*In vivo*, *in vitro* breast (MCF-7) cancer cells	132
$\mathbf{Ag_2S}$-MUA + Dox (covalent) + cRGD (covalent)	Dox	—/650 (830)	*In vivo*, *in vitro* breast (MCF-7) cancer cells	133
$\mathbf{Ag_2S}$-HS-PEG-COOH + FA (covalent) + Dox (non-covalent)	Dox	~13[b]/590 (775–930)	*In vitro*, carcinoma (HeLa) cancer cells	81
$\mathbf{Ag_2S}$-GSH + HOOC-PEG-FA (covalent) + Mtx (covalent)	Mtx	~114[b]/822	*In vitro*, cervical (HeLa), lung adenocarcinoma (A549), colon adenocarcinoma (HT29) cells	96
$\mathbf{Ag_{1.0}In_{3.2}S_{2.2}}$-GSH + HOOC-PEG-FA (covalent) + Mtx (covalent)	Mtx	~142[b]/634	*In vitro*, cervical (HeLa), lung adenocarcinoma (A549), colon adenocarcinoma (HT29) cells	96
$\mathbf{Ag_2S}$-2-MPA(PEI) + mPEG-OH (covalent) + H_2N-PEG-VA (covalent) + Cet (covalent) + 5-FU (non-covalent)	5-FU	~15[b]/807	*In vitro*, lung (A549, H1200) cancer cells	136
$\mathbf{Ag_2S}$-2-MPA + 5-FU (covalent) + H_2N-PEG-Cet (covalent) + ALA (non-covalent)	5-FU	114[b]/836	*In vitro*, colon adenocarcinoma (HCT116, SW480, HT29) cells	137
$\mathbf{AgInS_2}$-CMC + Cys (covalent) + KLA (covalent)	KLA	139[b]/660	*In vivo*, *in vitro* glioblastoma (U-87 MG, GBM) cells	140
$\mathbf{Ag_{1.0}In_{1.0}Zn_{1.0}S_{3.5}}$-MUA + Tf(covalent) + GA-Dox (covalent)	Dox	~11[b]/730	*In vitro*, lung carcinoma (H460) cells	142
$\mathbf{Ag_{1.0}In_{1.2}Zn_{5.6}S_{9.4}}$-MUA + FA (covalent) + Dox (covalent)	Dox	15.1[b]/576	*In vitro*, lung cancer (A549) cells	143
$\mathbf{Ag_{1.0}In_{6.8}Zn_{14.3}S_{154.2}}$-Cys + FA (covalent) + Dox (covalent)		17.6[b]/524		
$\mathbf{Ag_{1.0}In_{1.0}Zn_{8.8}S_{25.1}}$-DHLA + FA (covalent) + Dox (covalent)		22.5[b]/540		
$\mathbf{Ag_{1.0}In_{1.2}Zn_{5.6}S_{9.4}}$-MUA + β-CD (covalent) + FA (covalent) + UAs, C-2028 (non-covalent)	UAs	156[b]/576	*In vitro*, lung (H460) and prostate (Du-145, LNCaP) cancer cells	144, 145 and 146
$\mathbf{Ag_{1.0}In_{1.0}Zn_{1.0}S_{3.5}}$-MUA + β-CD (covalent) + FA (covalent) + UAs, C-2028 (non-covalent)		167[b]/730		

[a] Determined by SEM or TEM. [b] Determined by DLS, CMC – carboxymethylcellulose (M_w = 250 kDa), HOOC-PEG-COOH – dicarboxyl-terminated poly(ethylene glycol) (M_w = 2000), HA – hyaluronic acid, PBA – 3-carboxybenzeneboronic acid, cRGD – cyclo-(Arg–Gly–Asp–DTyr–Lys), HS-PEG-COOH – thiol and carboxyl-terminated poly(ethylene glycol) (M_w = 2000), GSH – 2-glutathione (tripeptide: γ-Glu–Cys–Gly), FA – folic acid, 2-MPA – 2-mercaptopropionic acid, PEI – branched polyethyleneimine (M_w = 25 kDa), mPEG-OH – methoxy(polyethylene glycol) (M_w = 2 kDa), H_2N-PEG-VA – amine–polyethylene glycol–valeric acid (M_w = 3.4 kDa), Cet – cetuximab (Erbitux®, C225), ALA – 5-aminolevulinic acid, MUA – 11-mercaptoundecanoic acid, Cys – L-cysteine, DHLA – dihydrolipoic acid, KLA – peptide (sequence LAKLAKKLAKLAK), Tf – transferrin, GA – glutaraldehyde, β-CD – β-cyclodextrin, Dox – doxorubicin, Tan – tangeretin, Que – quercetin, Mtx – methotrexate, 5-FU – 5-fluorouracil, UAs – unsymmetrical bisacridine derivatives.

covalent interactions or through covalent linkages. In **type C hybrids**, QDs stabilized with hydrophilic or hydrophobic ligands are subsequently encapsulated with polymers or copolymers of various types. It is challenging to define clear advantages or disadvantages for each hybrid type. From an economic perspective, considering the complexity of the hybrid system, **type A** is the most cost-effective, whereas **types B** and **C**, which involve the use of multiple reagents and synthetic methods, require significantly higher resources. On the other hand, **types B** and **C** benefit from the incorporation of targeting ligands, which enhances the efficient transport of the drug.

The next step involves appropriate modification of the hydrophilic layer of the capsule by introducing bioactive molecules. The drug is then introduced into the interior of the capsule or covalently bound to the capsule surface. The size of the resulting hybrids is most often estimated using the dynamic light scattering (DLS) technique, which allows for the determination of their hydrodynamic diameter (D_h). The colloidal stability of their dispersions can, in turn, be determined by measuring the zeta potential (ZP). It should be noted that an absolute value of this parameter, |ZP|, close to 30 mV or higher can be considered as a strong predictor of the high colloidal stability of the dispersion being investigated. The evaluation of hybrid systems in terms of their drug transport and release capabilities is typically performed by comparing drug release profiles at pH ~7 and pH ~5. These pH values serve as references for physiological (healthy cells) and tumor microenvironment conditions, respectively. It also is worth noting that nanocarriers exhibiting absorption and emission in the near-infrared (NIR) region, in addition to their potential application in bioimaging, can also be utilized in near-infrared photothermal therapy.

4.1. Type A hybrids

The simplest hybrid, consisting of QDs and a drug, was obtained by binding doxorubicin (Dox) to the surface of ZnO nanocrystals *via* electrostatic interactions. A rather low ZP

Table 3 Hybrid type C, composition, size, λ_{em} and applications

Hybrid composition – QD + ligands + drugs	Drug	Size(nm)/ λ_{em}(nm)	Applications	Ref.
Zn(Mn)S-NH_2 + NCA-L-Ala (polymerization) + Dextran (covalent) + Ibu (non-covalent, encapsulated)	Ibu	~45a/443 (585)	*In vitro*, human embryonic kidney (HEK293T) cells	158
InP/ZnS-MSC + CS-NHGs (non-covalent) + MUCAp (covalent) + SO + Ptx (non-covalent, encapsulated)	Ptx	20–50[a]/692 (696)	*In vitro* breast (MCF-7) cancer cells	161
Ag_2S-T-OA + CS (covalent) + Dox (non-covalent, encapsulated)	Dox	45–100[b]/ 1032	*In vivo*, *in vitro* colon (HeLa) cancer cells	162
Ag_2S-DDT + C18PMH/PEG (non-covalent) + Dox (non-covalent, encapsulated)	Dox	13.4[b]/1110	*In vivo*, *in vitro* breast (MDA-MB-231) cancer cells	164
Ag_2S-DDT + DSPE-PEG-COOH (non-covalent) + Ald (covalent) + Dox (non-covalent, encapsulated)	Ald, Dox	>100[b]/1150	*In vivo* bone tumor, *in vitro* lung carcinoma (A549) cells	166
Ag_2Se-DDT + DSPE-PEG-NH_2 (non-covalent) + heparin (covalent) + Dox (non-covalent, encapsulated) + SDF-1α (non-covalent)	Dox, SDF-1α	127[b]/1350	*In vivo*, *in vitro* breast (MDA-MB-231) cancer cells	167
$AgInS_2$/ZnS-DDT + PMAO (non-covalent) + Mtx (covalent)	Mtx	2.5[a]/530	*In vitro*, cervical (HeLa) cancer cells	168

[a] Determined by SEM or TEM. [b] Determined by DLS, NCA-L-Ala – cyclic monomer of L-alanine, Dextran – polysaccharide derived from the condensation of glucose, MSC – mercaptosuccinic acid, CS-NHGs – chitosan-based nanohydrogels, MUCAp – 3′-amino-modufied MUC aptamer (GCAGTTGATCCTTTGGATACCCTGG, 3′-amine, OD: 30), SO – sodium oxamate, T-OA – thiolated oleic acid, CS – chitosan (M_w = 21000), C18PMH/PEG – poly(maleic anhydride-*alt*-1-octadecene)-polyethylene glycol, DSPE-PEG-COOH – 1,2-distearoyl-*sn-glycero*-3-phosphoethanolamine-*N*-[carboxy(polyethylene glycol)], DSPE-PEG-NH_2 – 1,2-distearoyl-*sn-glycero*-3-phosphoethanolamine-*N*-[amino(polyethylene glycol)], Ibu – ibuprofen, Ptx – paclitaxel, Dox – doxorubicin, Ald – alendronate, SDF-1α – stromal cell-derived factor-1α, PMO – poly(maleic anhydride-*alt*-1-octadecene) (M_n = 30 000–50 000), Mtx – methotrexate.

value of −14.4 mV measured for ZnO nanocrystals was even lowered to −7.6 eV after the attachment of Dox.[124] Initial ZnO QDs and unbound Dox exhibited emission at 510 and 590 nm, respectively. Upon binding this drug to the nanocrystal surface fluorescence quenching occurred. According to the authors, this quenching resulted from the energy transfer from the ZnO to surface-bound Dox according to the mechanism discussed in one of the previous papers.[125] Moreover, it was shown that the luminescence properties were clearly dependent on pH. At pH = 7.5, emission quenching was observed, while upon its decrease to 5.0, a significant increase of red fluorescence originating from the "free" drug was visible since Dox was being slowly released from the surface of the hybrid undergoing decomposition in these conditions. ZnO–Dox hybrids were tested in *in vitro* studies on breast cancer cells.[124]

Another hybrid of A type containing amine-capped ZnO QDs was obtained through modification of the initial QDs with 3-aminopropyltriethoxysilane (APTES). Drug molecules – tangeretin (Tan) – were then non-covalently bound to the nanocrystal surface. The absorption spectrum of the unbound drug showed a band at 314 nm, while in the hybrid this band was shifted to 325 nm. The emission spectrum showed emission at 377 nm, 415 and 536 nm, solely originating from the ZnO-NH_2 QDs. For the ZnO-NH_2-Tan QDs hybrid, drug release profiles were determined at different pH values; at pH = 5.0, a significant increase in the release rate was observed compared to pH = 7.4. The hybrid system was tested in *in vitro* studies on lung cancer cells.[63]

In a ZnS QDs-based hybrid of type A, ZnS QDs were surface-functionalized with hydrophilic carboxymethylcellulose (CMC) ligands, which were introduced at the stage of the nanocrystal synthesis (primary ligands).[68] The obtained ZnS/CMC QDs dispersions exhibited high colloidal stability at pH = 7.0, as demonstrated by their ZP of −40 mV. At pH = 5.5, the ZP value switched to +35 mV. Upon doxorubicin molecule binding, the resulting ZnS/CMC-Dox hybrids showed a high ZP value of −42 mV. The hydrodynamic diameters of ZnS/CMC and ZnS/CMC-Dox were 29 and 58 nm, respectively. The initial ZnS/CMC nanocrystals and "free" Dox exhibited emission peaked at 426 and ~590 nm, respectively. In their hybrid both nanocrystal and Dox luminescence were quenched. The release profiles of Dox from the obtained ZnS/CMC-Dox hybrid were determined over time at a pH of 5.5, corresponding to cancer cells, and at pH = 7.2, corresponding to healthy ones.[126] The hybrid was tested in *in vitro* studies on brain cancer cells. In both cases (cancer and healthy cells), a similar rate of drug release was observed.[68]

MUA-capped hydrophilic colloidal Ag–In–Zn–S QDs of varying compositions were also tested as components of hybrids of type A.[127] In particular, nanocrystals of two different compositions were selected for the study, namely $Ag_{1.0}In_{1.2}Zn_{5.6}S_{9.4}$ and $Ag_{1.0}In_{1.0}Zn_{1.0}S_{3.5}$, emitting green (576 nm) and red (730 nm) light, respectively. Their primary ligands were exchanged for MUA. In the next step asymmetric bisacridine derivatives (UAs, C-2028 and C-2045, Fig. 2) were bound *via* noncovalent interactions, yielding, in total, four differently constructed hybrids.

The studied nanocrystals significantly differed in size (as determined by TEM), measuring approximately 3.1 and 5.8 nm, respectively. However, after the formation of their hybrids with drug molecules, DLS measurements showed similar D_h values for both nanocarriers which varied in the range of 9 to 13 nm, depending on the pH value (pH = 4.0, 5.5, 7.4 and 8.4). Their ZP values were also pH-dependent and negative in all cases, ranging from −5 to −40 mV. Their drug release profiles were determined at pH = 4.0 and 5.5, with the

greatest differentiation observed for the $Ag_{1.0}In_{1.0}Zn_{1.0}S_{3.5}$/MUA-C-2028 system. In summary, all hybrids exhibited high stability at pH = 7.4, while at lower pH levels of 5.5 and 4.0, release reaching 80% could be achieved. The obtained hybrid systems were tested in *in vivo* and *in vitro* studies on lung H460 and colon HCT116 cancer cells.[127,128]

Type A hybrids were also fabricated using carbon dots. Starting from bovine serum albumin (BSA) in ethanol, CDs with an average diameter of 6.8 nm and a hollow structure were synthesized *via* solvothermal carbonization, as confirmed by HRTEM analysis. Calculations based on the Barrett–Joyner–Halenda (BJH) model indicated that the hollow CDs (HCDs) possessed a specific surface area of 16.4 $m^2\ g^{-1}$ and a pore volume of $1.73 \times 10^{-2}\ cm^3\ g^{-1}$. These nanoparticles, exhibiting emission maxima at 460 and 440 nm, were subsequently functionalized with doxorubicin (Dox) through π–π stacking, hydrophobic interactions, and van der Waals forces. The pristine CDs displayed an average hydrodynamic diameter of 13 nm, as determined by dynamic light scattering (DLS), and a zeta potential (ZP) of −16.7 mV.

Upon Dox conjugation, the ZP decreased to −8.0 mV. In contrast, at pH = 5.0, the released fraction increased to 70%. The hybrid system was evaluated *in vitro* using A549 cells (human alveolar basal epithelial adenocarcinoma cells), HeLa cells (human cervical cancer cells), and MRC-5 cells (normal human fetal lung fibroblasts).[129] Another example of the application of CDs in the fabrication of type A hybrids was reported by H. U. Lee *et al.*[130] In their investigations, CDs were synthesized from cyanobacterial species collected from the Nakdong River in the southeastern region of Korea. The cyanobacteria dispersed in ethanol were subjected to ultrasonic treatment for 90 min. The obtained CDs exhibited average diameters of approximately 5.7 nm and were surfacially enriched with carboxyl groups, which ensured the stability of their aqueous dispersions and enabled drug conjugation. Doxorubicin (Dox) molecules were directly attached to these CDs. The resulting hybrids were evaluated *in vitro* using human hepatocellular carcinoma (HepG2) and human breast cancer (MCF-7) cell lines, as well as *in vivo* in a murine model. The studies demonstrated an enhanced anticancer effect compared with the administration of the free drug.[130]

4.2. Type B hybrids

Hybrids of type B are complex systems to which, in addition to the nanocarrier, ligands, and drug molecules, other components are also introduced. Their structural integrity is assured by both non-covalent and covalent interactions. Amine-capped ZnO-NH_2 QDs, obtained by reacting ZnO nanocrystals with 3-aminopropyltriethoxysilane (APTES), are most often used for the fabrication of this type of hybrid. In a procedure reported by X. Cai *et al.* a long-chain ligand, namely dicarboxyl-terminated poly(ethylene glycol), and a targeting ligand, hyaluronic acid (HA), were first attached to the ZnO-NH_2 QDs, in both cases by forming an amide bond in the reaction with 1-ethyl-3-(3-dimethylamino)propyl carbodiimide hydrochloride (EDC) and *N*-hydroxysuccinimide (NHS), as shown in Fig. 4a.[131] In the final step Dox was introduced into the system through non-covalent interactions. For the initial ZnO-NH_2 QDs, the measured ZP value was +27.4 mV, while after the introduction of the drug molecules it reversed the sign and lowered to −1.90 mV. They emitted green light with λ_{max} = 527 nm, whereas after the introduction of Dox, quenching of the emission at ∼590 nm characteristic of "free" Dox

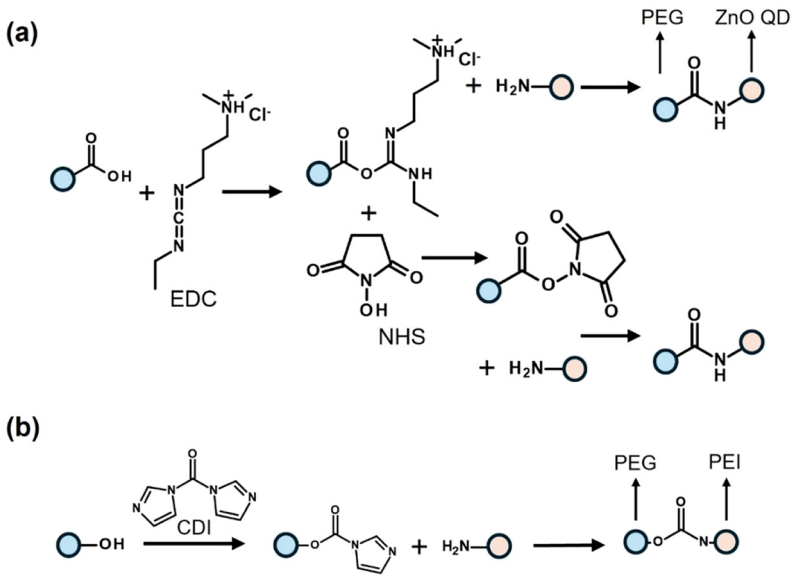

Fig. 4 (a) Chemical reaction scheme of EDC/NHS coupling of a carboxyl group on the ligand (bioactive compound) to a primary amine on the bioactive compound (ligand). (b) *N*,*N*′-Carbonyldiimidazole (CDI)-mediated coupling of a hydroxyl group on the polyethylene glycol to a primary amine on the ligand.

molecules was observed. Drug release profiles from the obtained hybrids were also determined, showing higher releases at pH = 5.0 compared to pH = 7.4. The hybrid system was tested in *in vitro* studies on lung (A549) cancer cells. A similar strategy was reported by Sadhukhan *et al.* who also used amine-capped ZnO-NH_2 QDs as initial nanocrystals.[132] 4-Carboxybenzeneboronic acid (PBA) molecules serving as *targeting ligands* were then grafted through the reaction with EDC/NHS resulting in the formation of an amide bond. In the second step, drug molecules – quercetin (Que) – were introduced *via* non-covalent interactions.

After adding subsequent hybrid components, the D_h value steadily increased, starting from ~140 nm for ZnO-NH_2 QDs, through ~280 nm for ZnO-PBA up to ~400 nm for ZnO-PBA QDs. The corresponding ZP values were +17.8 mV, −1.8 mV and −10.2 mV. Drug release profiles were determined for the obtained hybrids at different pH values; the highest releases were obtained at pH = 5.0 compared to pH = 6.0 and 7.4. The ZnO-PBA-Que QD hybrids were tested in *in vivo* and *in vitro* studies on breast (MCF-7) cancer cells.[132]

In the last decade, a number of articles were published focused on the application of Ag_2S QDs as drug nanocarriers. Chen *et al.* elaborated a new hybrid nanocarrier starting from hydrophilic Ag_2S nanocrystals capped with 3-MPA.[133] In the first step, drug molecules (Dox) were grafted to the ligand shell through amidation (EDC/NHS) involving the ligand carboxylic group and the drug amine group. In the second step, targeting ligands, namely cyclic RGD peptides (cRGD), were attached using the same reaction of the formation of an amide bond (EDC/NHS). The initial Ag_2S QDs and "free" Dox emitted light at 800 nm and ~590 nm, respectively. In the hybrid these bands were bathochromically shifted to 830 nm and 650 nm. The Ag_2S-(cRGD)-Dox QDs hybrid was tested in *in vivo* and *in vitro* studies on breast (MCF-7) cancer cells.[133] A similar strategy was proposed by Asik *et al.* who obtained hydrophilic Ag_2S QDs by introducing primary ligands in the form of a mixture of modified polyethylene glycols (PEGs): PEG-SH *i.e.* PEG containing an SH end group and HS-PEG-COOH *i.e.* PEG containing SH and COOH end groups.[81] In the next step, targeting ligands – folic acid (FA) – were attached, again by forming an amide bond (EDC/NHS) involving the carboxylic group of the hydrophilic ligand and the amino group of the FA. Finally, drug molecules (Dox) were introduced through non-covalent interactions. The initial Ag_2S QDs were very small (1.7–2.5 nm in size, as determined by TEM). The hydrodynamic diameter of the Ag_2S-PEG-FA-Dox hybrid reached a value of D_h = 10–13 nm (determined by DLS). Its ZP of −10.8 mV was relatively low. The initial Ag_2S QDs nanocrystals emitted radiation in the range of 775 to 930 nm, while the hybrid showed an additional emission band at ~590 nm attributed to Dox. The hybrid system was tested in *in vitro* studies on carcinoma (HeLa) cells.[81]

Hashemkhani *et al.* prepared a hybrid drug carrier starting from Ag_2S QDs stabilized with hydrophilic primary ligands (GSH).[96] Previously synthesized modified polyethylene glycol (HOOC-PEG-FA), containing a COOH group and an FA molecule at its ends, was then attached to the ligand shell *via* an amidation reaction (EDC/NHS) involving the amine group of the ligand (GSH) and the carboxylic group of the polymer. Drug molecules (methotrexate, Mtx) were subsequently grafted using the same type of amidation reaction (EDC/NHS). As determined by DLS measurements, D_h steadily increased with the grafting of each new component of the hybrid, changing from 30 nm for Ag_2S-GSH QDs to 76 nm for Ag_2S-GSH-PEG-FA QDs and finally to 114 nm for Ag_2S-GSH-PEG-FA-Mtx QDs. The corresponding changes in ZP were −21.5, −27.0 and −15.0 mV.

These authors applied the same procedure to prepare nanocarriers from ternary non-stoichiometric Ag–In–S QDs of composition $Ag_{1.0}In_{3.2}S_{2.2}$, also stabilized with GSH. The obtained Ag–In–S-GSH-PEG-FA-Mtx hybrids were characterized by D_h = 142 nm and ZP = −24.6 mV. The initial colloidal Ag_2S and $Ag_{1.0}In_{3.2}S_{2.2}$ nanocrystals used for the preparation of both types of hybrid exhibited emission at 822 and 634 nm, respectively. Upon grafting the targeting ligands and drug molecules, a partial quenching of emission was observed with a slight bathochromic shift. The drug release profiles determined for both hybrids showed low release at pH = 5.5 and 7.4, while a significant increase was observed at pH = 5.5 after laser illumination at 640 nm for 10 min at 37 °C, indicating their potential use in photothermal therapy. The hybrids also were tested in *in vitro* studies on cervical (HeLa) cancer, lung adenocarcinoma (A549), and colon adenocarcinoma (HT29) cells.[96]

An interesting hybrid was obtained by Duman *et al.* starting from Ag_2S QDs prepared in a mixture of 2-MPA and branched polyethyleneimine (BPEI).[134] In the first step, using the amine groups of the ligand (BPEI), mPEG-OH was attached by activating its hydroxyl groups with *N*,*N*′-carbonyldiimidazole (CDI) (Fig. 4b).[135] Then, in parallel, amine–polyethyleneglycol–valeric acid was grafted *via* an amidation reaction involving the amine groups of the ligand (BPEI) (EDC/NHS). In the second step, targeting ligands – cetuximab (Erbitux®, C225, Cet) were attached through terminal primary amine groups (PEG) forming an amide bond (EDC/NHS), while the drug – 5-fluorouracil (5-FU) – was introduced *via* non-covalent interactions in a buffer at pH = 7.4. The initial Ag_2S QDs were characterized by D_h = 7.4 nm and ZP = +11.8 mV. Upon formation of the hybrid D_h increased to 14.8 nm where the value of ZP dropped to +1.6 mV. The initial Ag_2S QDs emitted light at approximately 800 nm with a PLQY value of ~50%. In the hybrid the PLQY decreased to approximately 15%, with the emission wavelength essentially unchanged. The hybrid was tested *in vitro* on A549 and H1299 lung cancer cells.[136]

The same research group of Acar *et al.* designed a series of hybrids based on hydrophilic 2-MPA-capped Ag_2S QDs.[79,137] In the first step, 5-aminolevulinic acid (ALA), previously used in protoporphyrin-based photodynamic therapy, was attached to these Ag_2S QDs.[138,139] Three methods of ALA attachment were tested: through non-covalent electrostatic interactions at pH = 7.2–7.4 or *via* typical covalent grafting, either direct or indirect. The direct covalent attachment was achieved through amidation (EDC/sulfo-*N*-hydroxysuccinimide, sulfo-NHS), involving the carboxyl group of the ligand (2-MPA) and the amino group

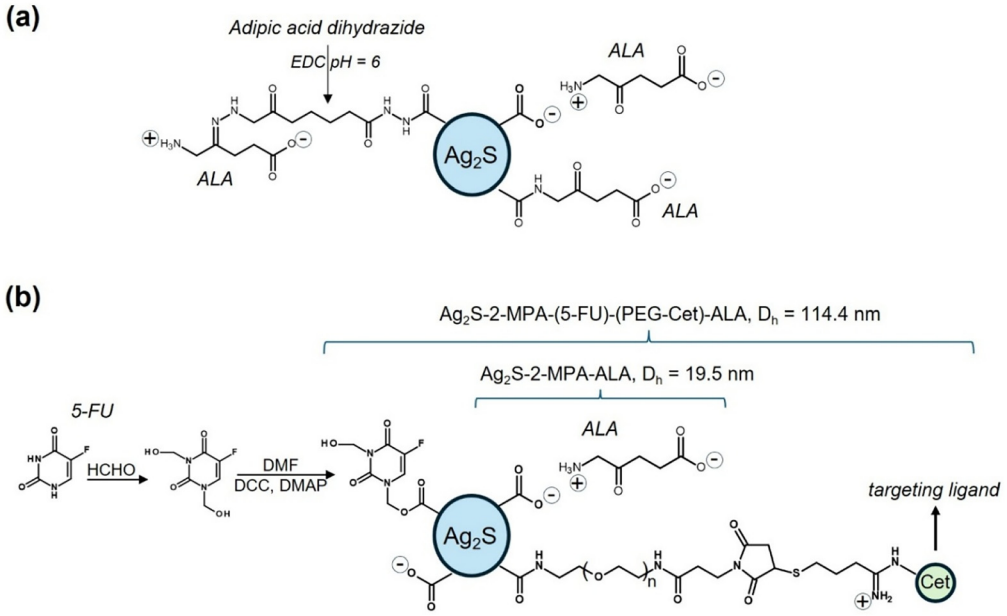

Fig. 5 (a) Different routes of ALA-conjugated Ag_2S-2-MPA QDs. (b) Schematic illustration of the construction of hybrids: Ag_2S-2-MPA-ALA and Ag_2S-2-MPA-(5-FU)-(PEG-Cet)-ALA.[137]

of ALA. In the indirect grafting a linker, namely adipic acid dihydrazide, was first attached to 2-MPA, and then ALA was grafted to it attached *via* a hydrazone linkage (Fig. 5a). The highest release of ALA at pH = 5.5, measured after 24 h, was observed for hybrids with electrostatically bound ALA (48%), and the lowest for the hybrid obtained by direct grafting (34%).[137] In the next stage of this research, a complex nanocarrier hybrid was elaborated, suitable for use in chemotherapy as well as photodynamic therapy. The drug (5-FU) was first transformed into its diol form in the reaction with formaldehyde. It was then grafted to the ligand shell *via* esterification carried out in the presence 4-dimethylaminopyridine (DMAP) and *N*,*N*′-dicyclohexylcarbodiimide (DCC). In the next step modified polyethylene glycol containing an amino group at one end and a targeting ligand – cetuximab (Erbitux®, C225, Cet) – at the other was attached to the ligand (2-MPA) *via* amidation (EDC/sulfo-NHS). In the final step, ALA was introduced *via* electrostatic interactions following previously developed procedures.[137] For the following hybrids Ag_2S-(2-MPA)-ALA and Ag_2S-(2-MPA)-(5-FU)-(PEG-Cet)-ALA (Fig. 5b), the measured D_h values were equal to 19.5 and 114.4 nm while the corresponding ZP values amounted to −13.6 and −7.8 mV, respectively.

The initial Ag_2S QDs exhibited emission at 830 nm which was slightly bathochromically shifted upon the formation of the hybrids. The hybrids were tested in *in vitro* studies on colon adenocarcinoma (HCT116, SW480 and HT29) cells.[137]

Hybrids containing ternary stoichiometric ($AgInS_2$) and non-stoichiometric (Ag–In–S) QDs were also developed. Mansur *et al.* prepared drug nanocarriers based on hydrophilic ternary $AgInS_2$ QDs obtained in the presence of carboxymethylcellulose (CMC).[140] L-Cysteine molecules, as cell-penetrating moieties, were first grafted to the ligand shell through amidation (EDC/NHS). In the next step, a mitochondria-targeting pro-apoptotic peptide (KLA) was attached to these L-cysteine-functionalized nanocrystals. The measured D_h value for the AgInS/CMC-Cys hybrid was equal to 66 nm. After KLA grafting to yield the AgInS/CMC-Cys-KLA hybrid it increased to 139 nm. The corresponding ZP values amounted to −18 and −13 mV, respectively. The initial $AgInS_2$ QDs exhibited emission at 660 nm, while a significant decrease of PLQY with a concomitant slight hypsochromic shift was observed in the spectra of the hybrids. The hybrids were tested in *in vivo* and *in vitro* studies on glioblastoma (U-87 MG, GBM) cells and malignant human brain HTB-14TM tumors.[140] Hydrophilic $AgInS_2$ QDs were synthesized from a mixture of simple precursors ($AgNO_3$ and $InCl_3$) in aqueous medium in the presence of polyethyleneimine (PEI) to which a Na_2S solution was introduced. They were employed as carriers for celastrol (Cel), a natural product isolated from the root of *Tripterygium wilfordii*.[141] Celastrol was conjugated to the surface of $AgInS_2$ QDs (2–4 nm in diameter) *via* direct amide bond formation. The resulting hybrid nanohybrids were evaluated *in vitro* in Hep3B and HepG2 hepatocellular carcinoma cell lines.[141]

Quaternary, nonstoichiometric Ag–In–Zn–S QDs also turned out to be promising components of type B hybrids. In this case nanocrystals capped with hydrophobic ligands were rendered hydrophilic through the exchange of primary ligands for hydrophilic ones such as MUA, Cys and DHLA.[100] These hydrophilic nanocrystals of the composition $Ag_{1.0}In_{1.0}Zn_{1.0}S_{3.5}$, stabilized with MUA, were then functionalized by attaching targeting ligands, namely transferrin (Tf), *via* amidation. The drug Dox, previously modified in a reaction with glutaraldehyde (GA), was then attached to this system through the for-

mation of an imine bond with Tf. The hydrodynamic diameter measured for $Ag_{1.0}In_{1.0}Zn_{1.0}S_{3.5}$-MUA was equal to *ca*. 9 nm. It increased to 11 nm for the final hybrid. The initial nanocrystals exhibited emission at 730 nm with a PLQY of 30%. After Tf grafting, a significant decrease in the value of PLQY to *ca.* 12% was observed. The hybrid system was tested in *in vitro* studies on lung carcinoma (H460) cells.[142]

Ruzycka-Ayoush *et al.* prepared three series of quaternary Ag–In–Zn–S nanocrystals differing in composition and capped with three different hydrophilic ligands MUA, Cys and DHL, namely $Ag_{1.0}In_{1.2}Zn_{5.6}S_{9.4}$-MUA, $Ag_{1.0}In_{6.8}Zn_{14.3}S_{154.2}$-Cys and $Ag_{1.0}In_{1.0}Zn_{8.8}S_{25.1}$-DHLA, characterized by emission at 576, 524 and 540 nm, respectively.[143] Targeting ligands – FA – were then grafted to the capping ligand shell through amidation (EDC/NHS) involving carboxylic groups of the ligands. In the next step Dox was attached, again by forming an amide bond (EDC/NHS). Two grafting sites were available in this case either *via* the ligand carboxylic group or *via* the carboxylic group of FA. The hydrodynamic diameters measured for the three resulting hybrids (AgInZnS-MUA-FA-DOX, AgInZnS-Cys-FA-Dox and AgInZnS-DHLA-FA-Dox) were 15.1, 17.6 and 22.5 nm, respectively. The corresponding ZP amounted to −15.5, −17.2 and −6.2 mV. All three types of hybrid were tested in *in vitro* studies on lung cancer (A549) cells.[143]

More complex hybrids were obtained using alloyed nanocrystals of the following compositions: $Ag_{1.0}In_{1.2}Zn_{5.6}S_{9.4}$-MUA and $Ag_{1.0}In_{1.0}Zn_{1.0}S_{3.5}$-MUA, both stabilized with MUA and characterized by green (576 nm) and red (730 nm) emission, respectively. In the first step β-cyclodextrin (β-CD) was attached to the capping ligands shell *via* esterification (EDC/DMAP) involving the carboxylic group of the ligand (MUA), to which targeting ligands (FA) were then grafted under the same conditions, again through esterification. In the next step, drug molecules, namely unsymmetrical bisacridine derivatives (UAs, C-2028, C-2045, Fig. 2 and 6) were introduced by forming an inclusion complex with β-CD (pocket size 7.9 × 7.0 Å). The D_h and ZP values determined for the initial nanocrystals were 9.9 nm and −37.5 mV for $Ag_{1.0}In_{1.2}Zn_{5.6}S_{9.4}$-MUA and 9.8 nm and −34.4 mV for $Ag_{1.0}In_{1.0}Zn_{1.0}S_{3.5}$-MUA. The formation of the final hybrids resulted in a large increase of D_h to 156 nm and 167 nm and a relatively small drop in their ZP values to −30.2 mV and −31.3 mV, respectively.[144] The obtained hybrids were tested in *in vitro* studies on lung (H460) and prostate (Du-145, LNCaP) cancer cells.[144–146]

Type B hybrids were also synthesized using carbon dots (CDs) instead of quantum dots (QDs) of inorganic semiconductors, as reported by M. Zheng *et al.*[147] In this study, citric acid was employed as a precursor of carbon and polyene polyamine (PEPA) as a surface passivation agent, following a modification of previously developed synthetic protocols.[148,149] In the first stage, CDs with an average diameter of approximately 2.3 nm were obtained. These nanoparticles exhibited a pronounced excitation-dependent emission behaviour, a phenomenon previously reported for selected types of CD.[150] Upon increasing the excitation wavelength from 380 to 520 nm, a bathochromic shift of the emission maximum was observed, spanning from 462 to 550 nm. The highest PLQY of 21% was recorded at the 380 nm excitation wavelength. In the subsequent stage, Pt(IV) complexes (Oxa(IV)-COOH) were covalently grafted to the CD surface *via* amide bond formation, employing EDC/sulfo-NHS coupling chemistry and taking advantage of the amino groups present on the CD surface. The zeta potential (ZP) of the pristine CDs was +24.02 mV, which decreased to +16.69 mV following drug conjugation. The resulting hybrids were evaluated *in vitro* using the human hepatocellular carcinoma cell line HepG2 and *in vivo* in a hepatocarcinoma 22 (H22) liver cancer model established in Chinese Kunming (KM) mice.[147]

L. Yang *et al.*[151] reported the one-pot hydrothermal synthesis of highly luminescent polyethylene glycol (PEG)-anchored carbon dots (CDs) using a mixture of citric acid, PEG-2000, and ethylenediamine in aqueous solution. The obtained CDs exhibited an average diameter of approximately 6.1 nm and were surface-functionalized with amino groups.

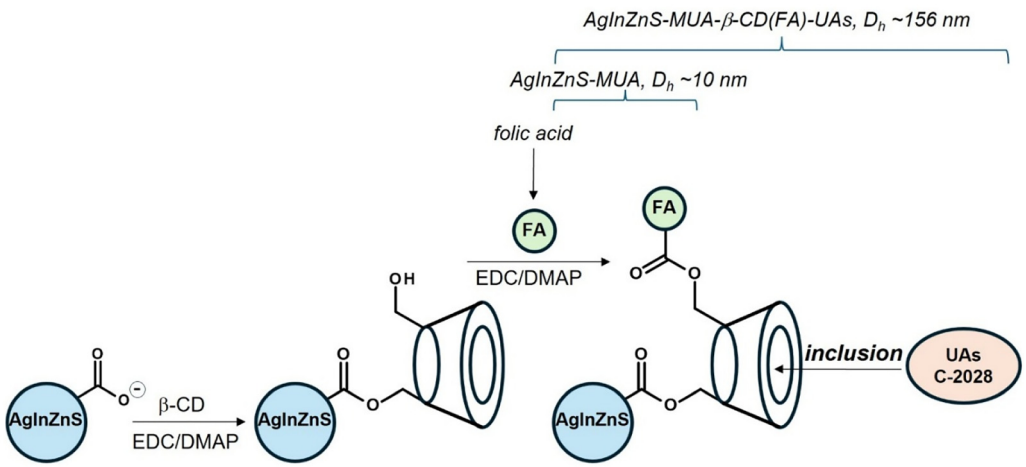

Fig. 6 Schematic illustration of the construction of a hybrid: AgInZnS-MUA-β-CD(-FA)-UAs-C-2028.[144]

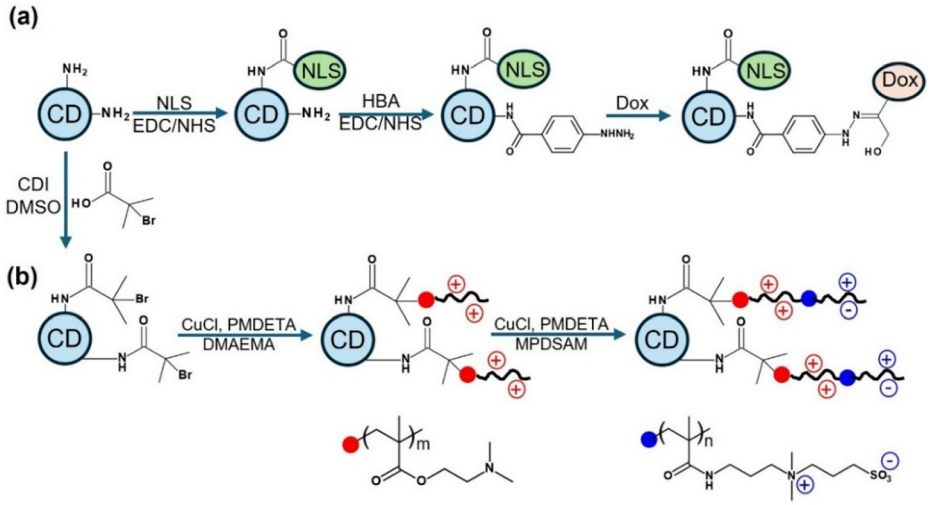

Fig. 7 Schematic illustration of the construction of hybrids: (a) CD-(NLS)-Dox,[152] and (b) CD-PDMA-PMPD.[153]

Exploiting the presence of these surface amine functionalities, targeting ligands in the form of a nuclear localization signal (NLS) peptide (T-antigen NLS, PKKKRKVG) were conjugated to the CD surface *via* EDC/NHS-mediated coupling chemistry.[151] In a subsequent study,[152] the same research group further modified the amine-functionalized CDs by covalently attaching 4-hydrazinobenzoic acid (HBA) through amide bond formation using EDC/NHS activation. Doxorubicin (Dox) molecules were then grafted to the hybrids *via* the formation of an acid-sensitive hydrazone bond between the terminal hydrazine groups derived from HBA and the carbonyl (ketone) group of Dox (Fig. 7a). The pristine CDs exhibited an emission maximum at approximately 450 nm, whereas the CD-(NLS)-Dox hybrid system displayed a fluorescence peak centred at 605 nm. The drug release profiles of the obtained hybrids clearly demonstrated a significantly higher percentage of drug release at pH 5.5 compared to physiological pH 7.4, confirming the pH-responsive behaviour of the hydrazone linkage. The hybrid nanoplatform was evaluated *in vitro* using human lung adenocarcinoma A549 cells and *in vivo* in an A549 xenograft nude mice model, confirming its potential for nucleus-targeted drug delivery and enhanced therapeutic efficacy.[152]

Another instructive example of type B hybrid design was reported by L. Cheng *et al.*[153] Starting from carbon dots (CDs) with diameters of approximately 2 nm, surface-functionalized with amino groups, the authors additionally introduced 2-bromoisobutyric acid moieties *via* amide bond formation. This functionalization enabled subsequent atom transfer radical polymerization (ATRP) from the CDs' surface. Through this strategy, a polycation-*b*-polysulfobetaine block copolymer, poly[2-(dimethylamino) ethyl methacrylate]-*b*-poly[*N*-(3-(methacryloylamino) propyl)-*N*,*N*-dimethyl-*N*-(3-sulfopropyl) ammonium hydroxide], was grafted onto the CDs (Fig. 7b). The hydrodynamic diameters of the pristine CDs and the resulting CD-PDMA-PMPD hybrids were 2.3 nm and 38.4 nm, respectively. Both CDs and CD-PDMA-PMPD exhibited excitation-dependent emission behavior, with fluorescence spanning from 455 to 600 nm upon excitation changing in the range of 310–530 nm. The obtained hybrids were capable of condensing plasmid DNA (pDNA) into stable nanoscale complexes and effectively protecting the genetic material from enzymatic degradation.[153]

4.3. Type C hybrids

Research on the encapsulation of colloidal QDs is inherently related to the attempts of applications of cadmium or lead chalcogenide nanocrystals in biomedical sciences. Initially its main goal was to reduce the toxicity of these nanocrystals. The first investigations involved the encapsulation of CdSe/ZnS QDs, stabilized with hydrophobic TOP/TOPO ligands, with a specially functionalized copolymer obtained from polyacrylic acid which was rendered amphiphilic through the transformation of 40% of its carboxylic groups, which were converted into hydrophobic moieties in a reaction with octylamine.[10]

A similar approach was used in the case of an alternating copolymer, namely poly(maleic anhydride-*alt*-1-tetradecene, PMO) (M_n = 7300, PDI ~1.23), to which, after hydrolysis, alkylamine groups were grafted in a reaction with bis(6-aminohexyl)amine.[11] Somehow more advanced encapsulation strategies involved the use of a triblock copolymer (M_w = 100 000) containing butyl and ethyl acrylate units (77%) and methacrylic acid units (23%) modified in a reaction with *n*-octylamine in the presence of EDC. After application of this copolymer for encapsulating QDs, the free carboxylic groups were reacted with amino-PEG, yielding hydrophilic chains.

The proposed approach allowed for the encapsulation of CdSe/ZnS QDs while maintaining their excellent luminescence properties. The measured PLQY values approached 60% practically across the entire pH range, from 0 to 14.[154] Encapsulation is one of the most effective methods for introducing quantum dots into aqueous environments without the necessity of exchanging hydrophobic ligands for hydrophilic

ones. This process is particularly advantageous in these cases in which the encapsulated nanocrystals retain the luminescence properties of nanocrystals capped with primary hydrophobic ligands. Furthermore, other molecules, such as *targeting ligands* and drugs, can be grafted to the surface of the capsules.

An interesting method for encapsulating Mn-doped ZnS QDs, synthesized according to the procedure described in reference, H. F. Wang *et al.*[67] Prior to encapsulation a cyclic monomer (NCA-L-Ala) was obtained in the reaction of L-alanine and triphosgene,[155,156] and then underwent a ring-opening polymerization reaction. The resulting polymer was then attached on one side to the ligand shell of the nanocrystal *via* an amino group, while terminating on its other side with another amino group. Dextran (M_n ~10 000), previously modified in reaction with chloroacetate, was then attached to this group by forming an amide bond.[157] In the next step ibuprofen (Ibu) molecules were attached to these encapsulated Mn-doped ZnS QDs, binding through the formation of hydrogen bonds between the –OH and –NH_2 groups of the polymer and the carboxylic groups of the drug, forming a noncovalent intermolecular complex.[155]

Fig. 8a schematically shows the constitution of the above-described hybrid. Its emission spectrum exhibited two bands at 443 and 585 nm originating from the nanocrystals. The determined drug release profiles indicated only a slightly higher release at pH = 7.4 as compared to pH = 5.0. The elaborated hybrids were tested in *in vitro* studies on human embryonic kidney (HEK293T) cells.[158]

In a different strategy, InP/ZnS QDs prepared according to the procedure described in ref. 74 were first transferred to water *via* exchange of primary ligands for mercaptosuccinic acid (MSA). They were then encapsulated with chitosan-based nanohydrogels (CS-NHGs) obtained from chitosan in the presence of a mixture of glacial acetic acid, *N*-isopropylacrylamide, *N*,*N*′-methylene bisacrylamide and ammonium persulfate.[159,160]

Encapsulation was carried out through vortexing and incubation of InP/ZnS QDs and CS-NHGs at 4 °C overnight, benefiting from CS-NHG swelling and physical incorporation of QDs capped with COOH-terminated ligands. Subsequently, targeting ligands, namely 3′-amino-modified MUC Ap, were attached to the surface of the capsules *via* amidation (EDC/NHS), while the drug, *i.e.* paclitaxel (Ptx), and sodium oxamate (SO) – a component improving the therapeutic effects – were incorporated into the capsules *via* noncovalent interactions in an overnight incubation process carried out at 4 °C. For the initial InP/ZnS QDs, two emission peaks were observed at 692 and

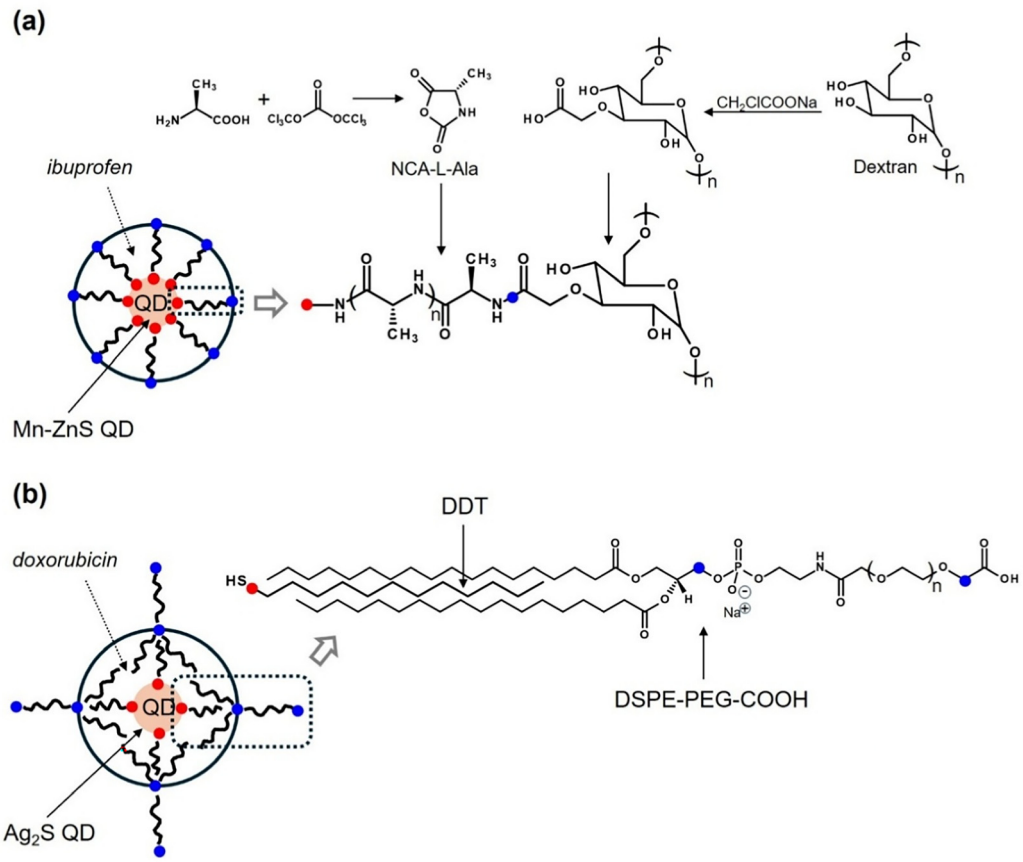

Fig. 8 Schematic illustration of the construction of hybrids: (a) Mn-ZnS QDs-poly(L-alanine)-Dextran-(Ibu-encapsulated),[158] and (b) Ag_2S QDs-DDT-DSPE-COOH-(Dox-encapsulated).[166]

698 nm, while upon encapsulation, the position of the first peak remained unchanged whereas the second underwent a slight hypsochromic shift to 696 nm. InP/ZnS QDs, initially rather small (sizes in the range from 1 to 5 nm, as determined by TEM), after encapsulation reached sizes ranging from 20 to 50 nm. Their drug release profiles indicated low release at pH = 7.4, which significantly increased at pH = 5.8. The hybrids were tested in *in vitro* studies on breast (MCF-7) cancer cells.[161]

Tan *et al.* investigated Ag_2S QDs as potential drug nanocarriers.[162] In their procedure the nanocrystals were first rendered hydrophilic through ligand exchange. In the next step they were encapsulated *via* the formation of amide-type bonds with chitosan. Drug (Dox) molecules were then introduced to the capsule through non-covalent interactions. Both the initial Ag_2S QDs and the hybrid emitted radiation at 1032 nm, with a PLQY value of ~13%. The initial Ag_2S QDs were characterized by D_h = 33.4 nm. Interestingly, the hybrid showed a dependence of D_h and ZP on pH. Changing pH from 7.4 to 5.0 resulted in an increase in D_h from ~50 nm to ~100 nm and an increase in ZP from +5 mV to +50 mV. This phenomenon was attributed to conformational changes in the polymeric (chitosan) capsules. The measured release profile showed increased Dox release at pH 5.0. The hybrid system was tested in *in vivo* and *in vitro* studies on colon cancer cells (HeLa).[162]

Encapsulation of colloidal Ag_2S QDs stabilized with hydrophobic ligands, namely DDT, was reported by Q. Wang *et al.*[29,76] A special amphiphilic copolymer (C18PMH/PEG) was prepared for this purpose by grafting polyethylene glycol side chains to poly(maleic anhydride-*alt*-1-octadecene, PMO), according to a procedure described in ref. 163. The presence of hydrophilic groups in the encapsulating polymer allowed for the ultrasound-assisted transfer of nanocrystals to aqueous media, without the necessity of exchanging the primary hydrophobic ligands for hydrophilic ones. In the last step molecules of the drug (Dox) were introduces to the capsule *via* non-covalent interactions. The initial Ag_2S-DDT QDs were rather small, characterized by a hydrodynamic diameter (D_h) of 3.6 nm, while for the hybrid D_h increased to 13.4 nm. The prepared hybrids emitted radiation at 1110 nm. The measured drug release significantly increased at pH = 5.5 compared to pH = 7.4, indicating the influence of the environment on drug binding within the capsule. The hybrids were tested in *in vivo* and *in vitro* studies on breast (MDA-MB-231) cancer cells.[164] H. Uludag reported on DDT-stabilized Ag_2S QDs, obtained under the same conditions as described above, which were, however, encapsulated differently.[165] Direct, ultrasound-assisted encapsulation was performed using 1,2-distearoyl-*sn-glycero*-3-phosphoethanolamine-*N*-[carboxy(polyethylene glycol)] (DSPE-PEG-COOH) (Fig. 8b). Alendronate (Ald) molecules, a clinical bisphosphonate drug for preventing osteolysis and alleviating pain, were then covalently attached to the capsule *via* amide bond formation (EDC/NHS). Doxorubicin (Dox) was non-covalently incorporated into the capsules. The resulting hybrid emitted radiation at 1150 nm, the emission at 590 nm, originating from Dox, being quenched. The drug release profiles determined for the hybrid system showed a significant increase in release from ~20% to ~80% upon lowering the pH from 7.4 to 5.0. The hybrids were tested in *in vivo* bone tumor and *in vitro* lung carcinoma (A549) studies.[166]

In the case of DDT-stabilized Ag_2Se QDs obtained according to the method developed by Dong *et al.* ultrasound-assisted encapsulation was performed using amino group-functionalized 1,2-distearoyl-*sn-glycero*-3-phosphoethanolamine-*N*-[amino(polyethylene glycol)] (DSPE-PEG-NH_2).[85] Heparin molecules were then grafted *via* amidation (EDC/NHS). In the next step doxorubicin (Dox) molecules were introduced into the polymer capsules. Finally, stromal cell-derived factor-1α (SDF-1α) was attached to the heparin by electrostatic adsorption. The resulting hybrids emitted radiation at 1350 nm characteristic of Ag_2Se QDs. The D_h of the initial nanocrystals was 4.3 nm, while for the hybrid system it increased to 127 nm. Release profiles were determined for both drugs. In the case of Dox, a significant increase of release was measured upon pH lowering from 7.4 to 5.5. For SDF-1α, low release was observed, practically independent of pH. The systems were tested in *in vivo* and *in vitro* studies on breast (MDA-MB-231) cancer cells.[167] Core/shell $AgInS_2$/ZnS QDs, stabilized with hydrophobic DDT ligands, were obtained according to a previously elaborated procedure.[97] In the next step they were encapsulated with poly(maleic anhydride-*alt*-1-octadecene) (PMO) copolymer and transferred to water under sonication. Subsequently, methotrexate (Mtx) drug molecules were grafted *via* amidation (EDC/NHS). The resulting hybrid exhibited emission at 530 nm originating from the QDs. It was tested in *in vitro* studies on cervical (HeLa) cancer cells.[168]

In the hybrid systems discussed above, colloidal QDs can be considered as central units to which individual elements of different functions are attached. It is, however, possible to use nanocrystals as elements of complex self-organized systems where they constitute one of several components. An instructive example of the approach is the elaboration of a tumor microenvironment-activated NIR-II nanotheranostic system for precise diagnosis and treatment of peritoneal metastases. The main advantage of systems of this type is the formation of a self-organizing, stable structure at pH ~7, corresponding to healthy cells, which disintegrates when the pH decreases in the presence of cancer cells. The FEAD1 system is a combination of five elements: **F**moc-His/**E**r^{3+}/**A**g_2S/**D**ox/**A1**904, as shown in Fig. 9.[169]

In the first stage of FEAD1 formation, Er^{3+} ions induce cross-linking between the histidine imidazole groups in Fmoc-His and the carboxylic groups of 3-MPA *i.e.* the ligand bound to the surface of the Ag_2S QDs.[170] In the second stage, Dox and the NIR absorber A1094,[171] acting as initiators, drive multicomponent self-assembly stabilized by intermolecular interactions, *i.e.*, hydrophobic interactions, π–π stacking, and electrostatic forces.[172–174] A regular globular aggregation of FEAD1 (95 nm in diameter) is formed at pH = 7.4 as evidenced by its TEM image. Its D_h amounts to approximately 120 nm and its ZP is rather low (approximately 18 mV). When the pH is decreased to 5.5, the TEM images show a disintegration of

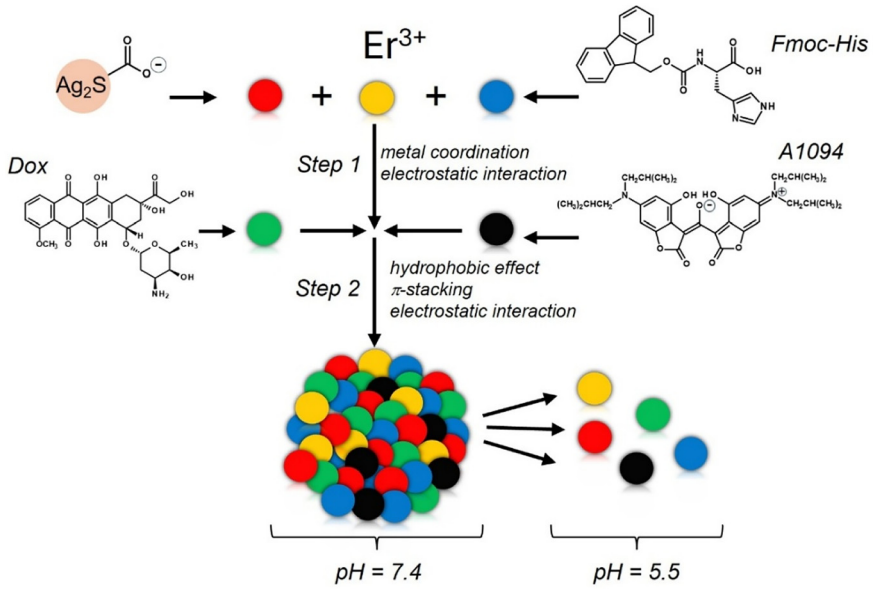

Fig. 9 Schematic illustration of the construction of the activatable NIR-II nanotheranostic system FEAD1.[169]

this aggregation. Simultaneously, D_h decreases to 34 nm. The photoluminescence of FEAD1 is extremely low, which is ascribed to quenching caused by Förster resonance energy transfer (FRET) between Ag_2S QDs emitting light at approximately 1200 nm and A1094. However, in acidic conditions FEAD1 fluorescence is restored through protonation of the imidazole groups in Fmoc-His and Dox, which weakens their coordination and hydrophobic interactions.[164,173] The FEAD1 system was tested in *in vivo* and *in vitro* studies on breast cancer cells (MDA-MB-231).[169]

5. Methods of the determination of drug content

In the studies of hybrid drug nanocarriers based on QDs, the amount of the incorporated drug is usually determined spectrophotometrically by applying the Beer–Lambert law. The relative drug content in the hybrid is most often characterized by two parameters, namely drug loading content (DLC) and drug entrapment efficiency (DEE), calculated according to eqn (1) and (2):

$$\mathrm{DLC}\,(\%) = \frac{\text{weight of drug in nanoparticles}}{\text{weight of nanoparticles taken}} \times 100\% \quad (1)$$

$$\mathrm{DEE}\,(\%) = \frac{\text{weight of drug in nanoparticles}}{\text{weight of drug injected}} \times 100\% \quad (2)$$

In the case of DLC, the amount of drug bound in the hybrid is most often expressed in relation to the mass of the nanocarrier; sometimes it is also expressed only in relation to the mass of the polymer constituting the capsule. The DEE parameter relates the amount of drug bound in the hybrid to the total amount of drug, which is usually the sum of bound and free drug. The ZnS-CMC-Dox hybrid can be considered here as an instructive example. In this hybrid the drug molecules were bound as a result of non-covalent interactions, and a value equivalent to DEE was determined from the formula $(A - B)/A$, where A (mg L^{-1}) is the initial concentration of Dox in the nanocarrier, and B (mg L^{-1}) is the concentration of Dox in the filtrate. The ZnS-CMC-Dox suspension was centrifuged using an ultracentrifuge filter with a 50 000 Da cut-off cellulose membrane.[68]

In many scientific reports, the authors do not provide a complete description of the procedure for determining the DEE parameter. The values of DLC and DEE can widely vary, and generally, the DLC value is significantly lower than that of DEE. For example, for a hybrid consisting of ZnO QDs capped with a polymeric ligands (HOOC-PEG-COOH), to which HA was covalently grafted and Dox introduced through non-covalent interaction, the DLC value reached only 30%, while the DEE value exceeded 80%.[131] Table 4 presents a comparison of DLC and DEE values for selected hybrid systems which do not contain toxic metals.

Dox in hybrid nanocarriers could also be determined electrochemically. In the case of hybrid Dox carriers consisting of quaternary Ag–In–Zn–S QDs functionalized with MUA and transferrin to which Dox was grafted, the amount of bound Dox was determined from the charge under the cathodic peak located at a potential of approximately −0.6 V *vs.* Ag/AgCl. Assuming a two-electron process (z = 2), the amount of Dox (m_{Dox}) was calculated using Faraday's law (eqn (3)):[142]

$$m_{Dox} = \frac{Q_{QD\text{-}Dox} \times M_{Dox}}{z \times F} \quad (3)$$

where: $Q_{QD\text{-}Dox}$ – the charge of the cathodic peak at the potential of approximately −0.6 V *vs.* Ag/AgCl, M_{Dox} – molecular

Table 4 Hybrid composition, drug, major absorption peak of drug, drug loading content (DLC) and entrapment efficiency (DEE)

Hybrid composition – QD + ligands + drug	Drug	λ_{ab} (nm)	DLC (%)	DEE (%)	Ref.
ZnS-CMC-Dox (non-covalent)	Dox	~490	—	99.0	68
ZnO-NH_2 + HOOC-PEG-COOH (covalent) + HA (covalent) + Dox (non-covalent)	Dox	~490	30.0	83.4	131
Ag_2S-T-OA + CS (covalent) + Dox (non-covalent, encapsulated)	Dox	~490	3.01–5.87	13.5–38.3	162
Ag_2S-DDT + C18PMH/PEG (non-covalent) + Dox (non-covalent, encapsulated)	Dox	~490	93.0	—	164
$Ag_{1.0}In_{1.2}Zn_{5.6}S_{9.4}$-MUA + FA (covalent) + Dox (covalent)	Dox	~490	4.6	—	143
$Ag_{1.0}In_{6.8}Zn_{14.3}S_{154.2}$-Cys + FA (covalent) + Dox (covalent)			5.4		
$Ag_{1.0}In_{1.0}Zn_{8.8}S_{25.1}$-DHLA + FA (covalent) + Dox (covalent)			3.9		
ZnO-NH_2 + PBA (covalent) + Que (non-covalent)	Que	378	31.8	46.7	132
Ag_2S-GSH + HOOC-PEG-FA (covalent) + Mtx (covalent)	Mtx	301	54.4	—	96
$Ag_{1.0}In_{3.2}S_{2.2}$-GSH + HOOC-PEG-FA (covalent) + Mtx (covalent)	Mtx	301	60.2	—	96
Ag_2S-2-MPA(PEI) + mPEG-OH (covalent) + H_2N-PEG-VA (covalent) + Cet (covalent) + 5-FU (non-covalent)	5-FU	265	7.3	57.8	136
Zn(Mn)S-NH_2 + NCA-L-Ala (polymerization) + Dextran (covalent) + Ibu (non-covalent, encapsulated)	Ibu	263	8.2–14.9	24.6–44.7	158
InP/ZnS-MSC + CS-NHGs (non-covalent) + MUCAp (covalent) + SO + Ptx (non-covalent, encapsulated)	Ptx	230	7.95–8.24	95.9–99.4	161

CMC – carboxymethylcellulose (M_w = 250 kDa), HOOC-PEG-COOH – dicarboxyl-terminated poly(ethylene glycol) (M_w = 2000), HA – hyaluronic acid, C18PMH/PEG – poly(maleic anhydride-*alt*-1-octadecene)-polyethylene glycol, MUA – 11-mercaptoundecanoic acid, Cys – L-cysteine, DHLA – dihydrolipoic acid, FA – folic acid, PBA – 3-carboxybenzeneboronic acid, GSH – 2-glutathione (tripeptide: γ-Glu–Cys–Gly), mPEG-OH – methoxy (polyethylene glycol) (M_w = 2 kDa), H_2N-PEG-VA – amine–polyethylene glycol–valeric acid (M_w = 3.4 kDa), Cet – cetuximab (Erbitux®, C225), NCA-L-Ala – cyclic monomer of L-alanine, Dextran – polysaccharide derived from the condensation of glucose, CS-NHGs – chitosan-based nanohydrogels, MUCAp – 3′-amino-modufied MUC aptamer (GCAGTTGATCCTTTGGATACCCTGG, 3′-amine, OD: 30), SO – sodium oxamate, Dox – doxorubicin, Que – quercetin, Mtx – methotrexate, 5-FU – 5-fluorouracil, Ibu – ibuprofen, Ptx – paclitaxel.

weight of Dox, z – number of electron (z = 2), F – Faraday constant.

This mass was 81 mg per 1 g of $Ag_{1.0}In_{1.0}Zn_{1.0}S_{3.5}$-transferrin, respectively.[142] In the same report, the maximum mass of drug per 1 g of the hybrid was estimated by calculating the maximum number of drug molecules from the ratio of the QD surface area (S_{QD}) to the drug surface area (S_{Dox}) according to eqn (4):

$$\text{Maximal number Dox per one QD} = \frac{S_{QD}}{S_{Dox}} = \frac{4 \times \pi \times {r_{QD}}^2}{\pi \times {r_{Dox}}^2} \quad (4)$$

where r_{QD} and r_{Dox} were determined from their D_h values measured by DLS measurements.

Based on the determined maximum amount of Dox, the mass of the drug per 1 g of QD was calculated. For the nanoconjugate $Ag_{1.0}In_{1.0}Zn_{1.0}S_{3.5}$-transferrin, this value was 136 mg of Dox per 1 g of the hybrid.[142] The electrochemical method can also be used for the determination of other drugs, such as unsymmetrical bisacridine derivatives (UAs = C-2028, C-2045, Fig. 2) non-covalently bound to the surface of $Ag_{1.0}In_{1.2}Zn_{5.6}S_{9.4}$ and $Ag_{1.0}In_{1.0}Zn_{1.0}S_{3.5}$ alloyed nanocrystals.[127]

The determination is based on the calculation of the charge (Q) by integrating the cathodic peak corresponding to the electroreduction of the nitro group in UAs. The mechanism of this process is strongly dependent on the pH of the electrochemical reaction medium.[175–177] In neutral aqueous media, the electroreduction of nitro groups is irreversible and involves the exchange of four electrons. The amount of drug (UAs) can be calculated using Faraday's formula according to eqn (3).

For example, in the case of a hybrid consisting of alloyed QDs of the formula $Ag_{1.0}In_{1.0}Zn_{1.0}S_{3.5}$ to which UAs were directly bound *via* non-covalent interactions the amounts of C-2028 and C-2045 determined electrochemically were 42.0 mg and 33.0 mg per 1 g of $Ag_{1.0}In_{1.0}Zn_{1.0}S_{3.5}$ QDs, respectively.[127] The same method was applied to hybrids composed of Ag–In–Zn–S QDs to which FA-functionalized β-CD molecules were attached, while the UA derivative C-2028 was introduced by inclusion to the cyclodextrin moiety. For C-2028, the drug mass was 4.74 mg per 1 g of quaternary, alloyed QDs of the composition $Ag_{1.0}In_{1.0}Zn_{1.0}S_{3.5}$.[144]

6. Summary and outlook

This critical review presents a detailed survey of strategies for designing different types of QD-based hybrid nanocarrier for drug delivery with a special emphasis on those which do not contain toxic metals. The described hybrids are characterized by varying degrees of complexity; moreover different types of covalent and coordination bond as well as non-covalent interaction are exploited to link the drug molecules to these nanocarriers. Among the numerous types of hybrid, relatively simple systems composed only of QDs and drug molecules bound non-covalently to them can be distinguished, as well as complex systems in which elaborate polymeric hydrophilic ligands are attached to the QD surface, providing, on the one hand, their colloidal dispersion stability, and on the other hand, the possibility of attaching drug molecules and other bioactive molecules such as targeting ligands.

The described hybrids have been primarily used as nanocarriers for doxorubicin, but also for other drugs. Considering current knowledge, the development of this domain of nanoscience is expected to proceed in two directions: (i) in the synthesis of hydrophilic inorganic semiconductor QDs characterized by emission in the NIR-II range and (ii) in the design

and fabrication of new hybrid systems capable of transporting a wide range of drugs.

Intensive research is expected in the development of new quantum dots suitable for drug delivery applications. The presence of toxic elements such as cadmium and lead in the nanocarrier is undeniably disqualifying for this type of application. However, the toxicity of other elements such as copper is debatable.[88]

Regarding emission in the NIR-II biological window, binary semiconductors with a band gap E_g < 1.0 eV, such as Ag_2S and Ag_2Se, are particularly interesting. Other potential inorganic semiconductors include InP ($E_{g(bulk)}$ = 1.35 eV, r_B = 10 nm), which is frequently tested in medical applications, and the significantly less popular InN with a distinctly smaller band gap ($E_{g(bulk)}$ = 0.7 eV, r_B = 8 nm).[178] Very promising are ternary semiconductors such as $AgInS_2$ and $AgInSe_2$, which, in combination with ZnS and ZnSe, can form core/shell type nanocrystals, as well as alloyed or non-stoichiometric quaternary Ag–In–Zn–S(Se) nanocrystals with tunable spectroscopic and redox properties.[90,179] In the domain of the design and preparation of hybrid systems, one of the most promising directions includes research devoted to the elaboration of complex systems such as FEAD1, *i.e.* a combination of several elements such as Fmoc-His/Er^{3+}/Ag_2S/Dox/A1904, including colloidal quantum dots, characterized by pH-dependent varying stability.[169] The investigation of the effect of pH on the stability of the ligand–drug molecule association is a crucial issue that applies to all newly designed hybrids.[180] In particular, the high stability of this association at pH ~7, together with its significant decrease at pH ~5, is a *sine qua non* condition of ensuring efficient drug delivery to cancer cells.

The vast majority of the elaborated hybrids were tested only in *in vitro* studies and were not further investigated in *in vivo* conditions. This approach focuses primarily on the immediate effects related to drug delivery to the cell but does not account for subsequent stages of transport, which involve a range of potentially beneficial and unfavorable processes. In this context, it is crucial to assess not only the stability of the entire hybrid but also that of its individual components, as well as their toxicity and potential accumulation in specific organs.

Abbreviations

Ala	L-Alanine
ALA	5-Aminolevulinic acid
Ald	Alendronate
AgTFA	Silver trifluoroacetate
ATRP	Atom transfer radical polymerization
APTES	3-Aminopropyltriethoxysilane
β-CD	β-Cyclodextrin
BPEI	Branched polyethylenimine
BSA	Bovine serum albumin
CCM	Cancer cell membranes
CDs	Carbon dots
CDI	*N*,*N*′-Carbonyldiimidazole
Cet	Cetuximab
CMC	Carboxymethylcellulose
cRGD	cyclo-(Arg–Gly–Asp–DTyr–Lys)
CS	Chitosan
Cys	L-Cysteine
DCC	*N*,*N*′-Dicyclohexylcarbodiimide
DDT	1-Dodecanethiol
DEE	Drug entrapment efficiency
D_h	Hydrodynamic diameter
DHLA	Dihydrolipoic acid
Dox	Doxorubicin
DLC	Drug loading content
DLS	Dynamic light scattering
DMAP	4-Dimethylaminopyridine
DMF	*N*,*N*-Dimethylformamide
EDC	1-Ethyl-3-(3-dimethylamino)propyl carbodiimide hydrochloride
E_g	Energy gap
$E_{g(bulk)}$	Bulk energy gap
EtOH	Ethanol
FA	Folic acid
5-FU	5-Fluorouracil
FWHM	Full width at half-maximum
GA	Glutaraldehyde
GR	Yeast glutathione reductase
GSH	Glutathione (γ-Glu–Cys–Gly)
HA	Hyaluronic acid
HBA	4-Hydrazinobenzoic acid
Ibu	Ibuprofen
ICG	Indocyanine green
$In(OAc)_3$	Indium acetate
$In(SA)_3$	Indium stearate
MA	Myristic acid
$Mg(OAc)_2$	Magnesium acetate
2-MPA	2-Mercaptopropionic acid
3-MPA	3-Mercaptopropic acid
MPTS	3-mercaptopropyltrimethoxysilane
MSA	Mercaptosuccinic acid
Mtx	Methotrexate
MUA	11-Mercaptoundecanoic acid
NADPH	Nicotinamide adenine dinucleotide phosphate
NHS	*N*-Hydroxysuccinimide
NIR-I	First biological window
NIR-II	Second biological window
NMP	*N*-Methylpyrrolidone
OA	Oleic acid
ODA	*n*-Octadecylamine
ODE	1-Octadecene
OLA	Oleylamine
LEDs	Light-emitting diodes
PAA	Poly(acrylic acid)
PBA	4-Carboxybenzeneboronic acid
PEI	Polyethyleneimine
PEPA	Polyene polyamine
PLQY	Photoluminescence quantum yield

PMO	Poly(maleic anhydride-*alt*-1-octadecene)
$P(TMS)_3$	Tris(trimethylsilyl)phosphine
Ptx	Paclitaxel
PVA	Polyvinyl alcohol
QDs	Quantum dots
Que	Quercetin
r_B	Bohr radius
SA	Stearic acid
SO	Sodium oxamate
Tan	Tangeretin
TEOS	Tetraethyl orthosilicate
Tf	Transferrin
TGA	Thioglycolic acid
$(TMS)_2S$	Hexamethyldisilathiane
TOP	Trioctylphosphine
UAs	Unsymmetrical bisacridine derivatives
$Zn(OAc)_2$	Zinc acetate
$Zn(SA)_2$	Zinc stearate
ZP	Zeta potential

Conflicts of interest

There are no conflicts to declare.

Data availability

No primary research results, software or code have been included, and no new data were generated or analysed as part of this review.

Acknowledgements

The authors want to acknowledge the support of the National Science Center of Poland, Grant No. 2022/45/B/ST5/02120.

References

1 A. I. Ekimov and A. A. Onushchenko, *Sov. Phys. Semicond.*, 1982, **16**, 775–777.
2 L. E. Brus, *J. Chem. Phys.*, 1984, **80**, 4403–4409.
3 C. B. Murray, D. J. Norris and M. G. Bawendi, *J. Am. Chem. Soc.*, 1993, **115**, 8706–8715.
4 S. C. Lims, N. A. Tran, V.-D. Dao and P. V. Pham, *Coord. Chem. Rev.*, 2025, **528**, 216423.
5 V. L. Colvin, M. C. Schlamp and A. P. Alivisatos, *Nature*, 1994, **370**, 354–357.
6 M. Bruchez, M. Moronne, P. Gin, S. Weiss and A. P. Alivisatos, *Science*, 1998, **281**, 2013–2016.
7 W. C. W. Chan and S. Nie, *Science*, 1998, **281**, 2016–2018.
8 M. Derfus, W. C. W. Chan and S. N. Bhatia, *Nano Lett.*, 2004, **4**, 11–18.
9 C. Kirchner, T. Liedl, S. Kudera, T. Pellegrino, A. M. Javier, H. E. Gaub, S. Stölzle, N. Fertig and W. J. Parak, *Nano Lett.*, 2005, **5**, 331–338.
10 X. Wu, H. Liu, J. Liu, K. N. Haley, J. A. Treadway, J. P. Larson, N. Ge, F. Peale and M. P. Bruchez, *Nat. Biotechnol.*, 2003, **21**, 41–46.
11 T. Pellegrino, L. Manna, S. Kudera, T. Liedl, D. Koktysh, A. L. Rogach, S. Keller, J. Rädler, G. Natile and W. J. Parak, *Nano Lett.*, 2004, **4**, 703–707.
12 L. Ye, K.-T. Yong, L. Liu, I. Roy, R. Hu, J. Zhu, H. Cai, W.-C. Law, J. Liu, K. Wang, J. Liu, Y. Liu, Y. Hu, X. Zhang, M. T. Swihart and P. N. Prasad, *Nat. Nanotechnol.*, 2012, **7**, 453–458.
13 G. Hong, S. Diao, A. L. Antaris and H. Dai, *Chem. Rev.*, 2015, **115**, 10816–10906.
14 A. Deb and D. Chowdhury, *Curr. Med. Chem.*, 2024, **31**, 3899–3924.
15 M. Smith, M. C. Mancini and S. Nie, *Nat. Nanotechnol.*, 2009, **4**, 710–711.
16 K. Welsher, Z. Liu, S. P. Sherlock, J. T. Robinson, Z. Chen, D. Daranciang and H. Dai, *Nat. Nanotechnol.*, 2009, **4**, 773–780.
17 G. Hong, S. Diao, J. Chang, A. L. Antaris, C. Chen, B. Zhang, B. Zhao, D. N. Atochin, P. L. Huang, K. I. Andreasson, C. J. Kuo and H. Dai, *Nat. Photonics*, 2014, **8**, 723–730.
18 S. Diao, G. Hong, A. L. Antaris, J. L. Blackburn, K. Cheng, Z. Cheng and H. Dai, *Nano Res.*, 2015, **8**, 3027–3034.
19 M. G. Bawendi, M. L. Steigerwald and L. E. Brus, *Annu. Rev. Phys. Chem.*, 1990, **41**, 477–496.
20 A. P. Alivisatos, *J. Phys. Chem.*, 1996, **100**, 13226–13239.
21 P. Reiss, M. Protière and L. Li, *Small*, 2009, **5**, 154–168.
22 O. Yarema, M. Yarema and V. Wood, *Chem. Mater.*, 2018, **30**, 1446–1461.
23 H. Zhong, Z. Bai and B. Zou, *J. Phys. Chem. Lett.*, 2012, **3**, 3167–3175.
24 A. D. P. Leach and J. E. Macdonald, *J. Phys. Chem. Lett.*, 2016, **7**, 572–583.
25 A. M. Smith and S. Nie, *Acc. Chem. Res.*, 2010, **43**, 190–200.
26 J. L. Shay, B. Tell, L. M. Schiavone, H. M. Kasper and F. Thiel, *Phys. Rev. B*, 1974, **9**, 1719–1723.
27 Y. J. Park, J. H. Oh, N. S. Han, H. C. Yoon, S. M. Park, Y. R. Do and J. K. Song, *J. Phys. Chem. C*, 2014, **118**, 25677–25683.
28 M. Green, *Curr. Opin. Solid State Mater. Sci.*, 2002, **6**, 355–363.
29 Y. Zhang, Y. Liu, C. Li, X. Chen and Q. Wang, *J. Phys. Chem. C*, 2014, **118**, 4918–4923.
30 A. Sahu, L. Qi, M. S. Kang, D. Deng and D. J. Noris, *J. Am. Chem. Soc.*, 2011, **133**, 6509–6512.
31 A. Sahu, A. Khare, D. D. Deng and D. J. Norris, *Chem. Commun.*, 2012, **48**, 5458–5460.
32 L. Li and P. Reiss, *J. Am. Chem. Soc.*, 2008, **130**, 11588–11589.
33 M. D. Tessier, D. Dupont, K. De Nolf, J. De Roo and Z. Hens, *Chem. Mater.*, 2015, **27**, 4893–4898.

34 S. Kim, T. Kim, M. Kang, S. K. Kwak, T. W. Yoo, L. S. Park, I. Yang, S. Hwang, J. E. Lee, S. K. Kim and S.-W. Kim, *J. Am. Chem. Soc.*, 2012, **134**, 3804–3809.
35 T. Torimoto, T. Adachi, K.-i. Okazaki, M. Sakuraoka, T. Shibayama, B. Ohtani, A. Kudo and S. Kuwabata, *J. Am. Chem. Soc.*, 2007, **129**, 12388–12389.
36 G. Gabka, P. Bujak, K. Giedyk, A. Ostrowski, K. Malinowska, J. Herbich, B. Golec, I. Wielgus and A. Pron, *Inorg. Chem.*, 2014, **53**, 5002–5012.
37 P. Kowalik, P. Bujak, M. Penkala, A. M. Maroń, A. Ostrowski, A. Kmita, M. Gajewska, W. Lisowski, J. W. Sobczak and A. Pron, *Chem. Mater.*, 2022, **34**, 809–825.
38 J. Krustok, J. Raudoja, M. Krunks, H. Mändar and H. Colla, *J. Appl. Phys.*, 2000, **88**, 205–209.
39 S. L. Castro, S. G. Bailey, R. P. Raffaelle, K. K. Banger and A. F. Hepp, *J. Phys. Chem. B*, 2004, **108**, 12429–12435.
40 H. Zhong, Y. Zhou, M. Ye, Y. He, J. Ye, C. He, C. Yang and Y. Li, *Chem. Mater.*, 2008, **20**, 6434–6443.
41 L. Li, T. J. Daou, I. Texier, T. T. K. Chi, N. Q. Liem and P. Reiss, *Chem. Mater.*, 2009, **21**, 2422–2429.
42 A. Ćwilich, D. Larowska-Zarych, P. Kowalik, L. Polok, P. Bujak, M. Duda, T. Kazimerczuk, W. Gadomski, A. Pron and Ł. Kłopotowski, *J. Phys. Chem. Lett.*, 2024, **15**, 10479–10487.
43 G. Xu, S. Zeng, B. Zhang, M. T. Swihart, K.-T. Yong and P. N. Prasad, *Chem. Rev.*, 2016, **116**, 12234–12327.
44 K. J. McHugh, L. Jing, A. M. Berhrens, S. Jayawardena, W. Tang, M. Gao, R. Langer and A. Jaklenec, *Adv. Mater.*, 2018, **30**, 1706356.
45 C. Li, G. Chen, Y. Zhang, F. Wu and Q. Wang, *J. Am. Chem. Soc.*, 2020, **142**, 14789–14804.
46 C. Ding, Y. Huang, Z. Shen and X. Chen, *Adv. Mater.*, 2021, **33**, 2007768.
47 Z. Piao, D. Yang, Z. Cui, H. He, S. Mei, H. Lu, Z. Fu, L. Wang, W. Zhang and R. Guo, *Adv. Funct. Mater.*, 2022, **32**, 2207662.
48 B. Chang, J. Chen, J. Bao, T. Sun and Z. Chen, *Chem. Rev.*, 2023, **123**, 13966–14037.
49 A. N. Goldstein, C. M. Echer and A. P. Alivisatos, *Science*, 1992, **256**, 1425–1427.
50 L. Jing, S. V. Kershaw, Y. Li, X. Huang, Y. Li, A. L. Rogach and M. Gao, *Chem. Rev.*, 2016, **116**, 10623–10730.
51 A. Heuer-Jungemann, N. Feliu, I. Bakaimi, M. Hamaly, A. Alkilany, I. Chakraborty, A. Masood, M. F. Casula, A. Kostopoulou, E. Oh, K. Susumu, M. H. Stewart, I. L. Medintz, E. Stratakis, W. J. Parak and A. G. Kanaras, *Chem. Rev.*, 2019, **119**, 4819–4880.
52 S. K. Golombek, J.-N. May, B. Theek, L. Appold, N. Drude, F. Kiessling and T. Lammers, *Adv. Drug Delivery Rev.*, 2018, **130**, 17–38.
53 E.-Q. Song, Z.-L. Zhang, Q.-Y. Luo, W. Lu, Y.-B. Shi and D.-W. Pang, *Clin. Chem.*, 2009, **55**, 955–963.
54 Y. Yu, J. Wang, S. C. Kaul, R. Wadhwa and E. Miyako, *Front. Oncol.*, 2019, **9**, 602.
55 K. R. Kampen, *J. Membr. Biol.*, 2011, **242**, 69–74.
56 P. Singh, R. K. Singh and R. Kumar, *RSC Adv.*, 2021, **11**, 2512–2545.
57 Y. Kayanuma, *Phys. Rev. B*, 1988, **38**, 9797–9805.
58 A. D. Yoffe, *Adv. Phys.*, 1993, **42**, 173–262.
59 F. Muhammad, M. Guo, W. Qi, F. Sun, A. Wang, Y. Guo and G. Zhu, *J. Am. Chem. Soc.*, 2011, **133**, 8778–8781.
60 F. Muhammad, M. Guo, Y. Guo, W. Qi, F. Qu, F. Sun, H. Zhao and G. Zhu, *J. Mater. Chem.*, 2011, **21**, 13406–13412.
61 J. Bang, H. Yang and P. H. Holloway, *Nanotechnology*, 2006, **17**, 973–978.
62 J. Zhang, D. Wu, M.-F. Li and J. Feng, *ACS Appl. Mater. Interfaces*, 2015, **7**, 26666–26673.
63 A. Roshini, S. Jagadeesan, L. Arivazhagan, Y.-J. Cho, J.-H. Lim, Y.-H. Doh, S.-J. Kim, J. Na and K. H. Choi, *Mater. Sci. Eng., C*, 2018, **92**, 477–488.
64 J.-H. Lin, E. A. Patil, R. S. Devan, Z.-A. Liu, Y.-P. Wang, C.-H. Ho, Y. Liou and Y.-R. Ma, *Sci. Rep.*, 2014, **4**, 6967.
65 A. Grala, M. Wolska-Pietkiewicz, W. Danowski, Z. Wróbel, J. Grzonka and J. Lewiński, *Chem. Commun.*, 2016, **52**, 7340–7343.
66 M. Jędrzejewska, M. Wolsko-Pietkiewicz, Z. Drużyński and J. Lewiński, *J. Mater. Chem. C*, 2023, **11**, 15016–15029.
67 H.-F. Wang, Y. He, T.-R. Ji and X.-P. Yan, *Anal. Chem.*, 2009, **81**, 1615–1621.
68 A. A. P. Mansur, A. J. Caires, S. M. Carvalho, N. S. V. Capanema, I. C. Carvalho and H. S. Mansur, *Colloids Surf., B*, 2019, **184**, 110507.
69 S. Tamang, G. Beaune, I. Texier and P. Reiss, *ACS Nano*, 2011, **5**, 9392–9402.
70 P. Bujak, *Synth. Met.*, 2016, **222**, 93–114.
71 D. Battaglia and X. Peng, *Nano Lett.*, 2002, **2**, 1027–1030.
72 L. Li, M. Protière and P. Reiss, *Chem. Mater.*, 2008, **20**, 2621–2623.
73 M. D. Tessier, D. Dupont, K. De Nolf, J. De Roo and Z. Hens, *Chem. Mater.*, 2015, **27**, 4893–4898.
74 R. Xie, D. Battaglia and X. Peng, *J. Am. Chem. Soc.*, 2007, **129**, 15432–15433.
75 R. Gui, H. Jin, Z. Wang and L. Tan, Recent advances in synthetic methods and applications of colloidal silver chalcogenide quantum dots, *Coord. Chem. Rev.*, 2015, **296**, 91–124.
76 Y. Du, B. Xu, T. Fu, M. Cai, F. Li, Y. Zhang and Q. Wang, *J. Am. Chem. Soc.*, 2010, **132**, 1470–1471.
77 P. Jiang, Z.-Q. Tian, C.-N. Zhu, Z.-L. Zhang and D.-W. Pang, *Chem. Mater.*, 2012, **24**, 3–5.
78 Y. Zhang, G. Hong, Y. Zhang, G. Chen, F. Li, H. Dai and Q. Wang, *ACS Nano*, 2012, **6**, 3695–3702.
79 I. Hocaoglu, M. N. Çizmeciyan, R. Erdem, C. Ozen, A. Kurt, A. Sennaroglu and H. Y. Acar, *J. Mater. Chem.*, 2012, **22**, 14674–14681.
80 M. Hashemkhani, K. Bilici, A. Muti, A. Sennaroglu and H. Y. Acar, *New J. Chem.*, 2020, **44**, 5419–5427.
81 D. Asik, M. B. Yagci, D. Duman and H. Y. Acar, *J. Mater. Chem. B*, 2016, **4**, 1941–1950.

82 O. El-Dahshan, A. Daniaud, W. L. Ling, K. D. Wegner, O. Proux, G. Veronesi and P. Reiss, *Nanoscale*, 2025, **17**, 14637–14646.
83 M. Yarema, S. Pichler, M. Sytnyk, R. Seyrkammer, R. T. Lechner, G. Fritz-Popovski, D. Jarzab, K. Szendrei, R. Resel, O. Korovyanko, M. A. Loi, O. Paris, G. Hesser and W. Heiss, *ACS Nano*, 2011, **5**, 3758–3765.
84 C.-N. Zhu, P. Jiang, Z.-L. Zhang, D.-L. Zhu, Z.-Q. Tian and D.-W. Pang, *ACS Appl. Mater. Interfaces*, 2015, **5**, 1186–1189.
85 B. Dong, C. Li, G. Chen, Y. Zhang, Y. Zhang, M. Deng and Q. Wang, *Chem. Mater.*, 2013, **25**, 2503–2509.
86 Y.-P. Gu, R. Cui, Z.-L. Zhang, Z.-X. Xie and D.-W. Pang, *J. Am. Chem. Soc.*, 2012, **134**, 79–82.
87 B. Nowack, *Science*, 2010, **330**, 1054–1055.
88 J. C. Kays, A. M. Saeboe, R. Toufanian, D. E. Kurant and A. M. Dennis, *Nano Lett.*, 2020, **20**, 1980–1991.
89 D. Aldakov, A. Lefrançois and P. Reiss, *J. Mater. Chem. C*, 2013, **1**, 3756–3776.
90 D. Moodelly, P. Kowalik, P. Bujak, A. Pron and P. Reiss, *J. Mater. Chem. C*, 2019, **7**, 11665–11709.
91 P. M. Allen and M. G. Bawendi, *J. Am. Chem. Soc.*, 2008, **130**, 9240–9241.
92 O. Yarema, M. Yarema, D. Bozyigit, W. M. M. Lin and V. Wood, *ACS Nano*, 2015, **9**, 11134–11142.
93 D. Deng, L. Qu and Y. Gu, *J. Mater. Chem. C*, 2014, **2**, 7077–7085.
94 X. Kang, Y. Yang, L. Huang, Y. Tao, L. Wang and D. Pan, *Green Chem.*, 2015, **17**, 4482–4488.
95 M. Dai, S. Ogawa, T. Kameyama, K.-i. Okazaki, A. Kudo, S. Kuwabata, Y. Tsuboi and T. Torimoto, *J. Mater. Chem.*, 2012, **22**, 12851–12858.
96 M. Hashemkhani, A. Muti, A. Sennaroğlu and H. Y. Acar, *J. Photochem. Photobiol., B*, 2020, **213**, 112082.
97 J.-Y. Chang, G.-Q. Wang, C.-Y. Cheng, W.-X. Lin and J.-C. Hsu, *J. Mater. Chem.*, 2012, **22**, 10609–10618.
98 G. Gabka, P. Bujak, K. Kotwica, A. Ostrowski, W. Lisowski, J. W. Sobczak and A. Pron, *Phys. Chem. Chem. Phys.*, 2017, **19**, 1217–1228.
99 P. Bujak, Z. Wróbel, M. Penkala, K. Kotwica, A. Kmita, M. Gajewska, A. Ostrowski, P. Kowalik and A. Pron, *Inorg. Chem.*, 2019, **58**, 1358–1370.
100 P. Kowalik, P. Bujak, M. Penkala and A. Pron, *Nanomaterials*, 2021, **11**, 843.
101 P. Kowalik, P. Bujak, M. Penkala, W. Tomaszewski, W. Lisowski, J. W. Sobczak, D. Siepietowska, A. M. Maroń, J. Polak, M. Bartoszek and A. Pron, *Chem. Mater.*, 2023, **35**, 6447–6462.
102 M. Mrad, T. B. Chaabane, H. Rinnert, B. Lavinia, J. Jasniewski, G. Medjahdi and R. Schneider, *Inorg. Chem.*, 2020, **59**, 6220–6231.
103 Y. Sheng, X. Tang and J. Xue, *J. Mater. Chem.*, 2012, **22**, 1290–1296.
104 S. Y. Lim, W. Shen and Z. Gao, *Chem. Soc. Rev.*, 2015, **44**, 362–381.
105 S. Ding, M. Zhou, A. B. Isaev, N. Meng, X. Zhang, L. Ma and W. Wang, *Coord. Chem. Rev.*, 2025, **544**, 216956.
106 X. Xu, R. Ray, Y. Gu, H. J. Ploehn, L. Gearheart, K. Raker and W. A. Scrivens, *J. Am. Chem. Soc.*, 2004, **126**, 12736–12737.
107 Y.-P. Sun, B. Zhou, Y. Lin, W. Wang, K. A. S. Fernando, P. Pathak, M. K. Meziani, B. A. Harruff, X. Wang, H. Wang, P. G. Luo, H. Yang, M. E. Kose, B. Chen, L. M. Veca and S.-Y. Xie, *J. Am. Chem. Soc.*, 2006, **128**, 7756–7757.
108 K. Jiang, S. Sun, L. Zhang, Y. Lu, A. Wu, C. Cai and H. Lin, *Angew. Chem., Int. Ed.*, 2015, **54**, 5360–5363.
109 L. Wang, W. Li, L. Yin, Y. Liu, H. Guo, J. Lai, Y. Han, G. Li, J. Zhang, R. Vajtai, P. M. Ajayan and M. Wu, *Sci. Adv.*, 2020, **6**, eabb6772.
110 Y. Deng, D. Zhao, X. Chen, F. Wang, H. Song and D. Zhen, *Chem. Commun.*, 2013, **49**, 5751–5753.
111 S. Zhou, F. Wang, N. Feng, A. Xu, X. Sun, J. Zhou and H. Li, *Small*, 2023, **19**, 2301240.
112 B. Geng, J. Hu, Y. Li, S. Feng, D. Pan, L. Feng and L. Shen, *Nat. Commun.*, 2022, **13**, 5735.
113 S. Patil and R. Chandrasekaran, *J. Genet. Eng. Biotechnol.*, 2020, **18**, 67.
114 K. Bloch, B. Sarkar and S. Ghosh, *Curr. Microbiol.*, 2024, **81**, 294.
115 Z. L. Wu, P. Zhang, M. X. Gao, C. F. Liu, W. Wang, F. Leng and C. Z. Huang, *J. Mater. Chem. B*, 2013, **1**, 2868–2873.
116 S. Sahu, B. Behera, T. K. Maiti and S. Mohapatra, *Chem. Commun.*, 2012, **48**, 8835–8837.
117 B. De and N. Karak, *RSC Adv.*, 2013, **3**, 8286–8290.
118 L. Wu, M. Luderer, X. Yang, C. Swain, H. Zhang, K. Nelson, A. J. Stacy, B. Shen, G. M. Lanza and D. Pan, *Theranostics*, 2013, **3**, 677–686.
119 L. Wu, X. Cai, K. Nelson, W. Xing, J. Xia, R. Zhang, A. J. Stacy, M. Luderer, G. M. Lanza, L. V. Wang, B. Shen and D. Pan, *Nano Res.*, 2013, **6**, 312–325.
120 S. Y. Park, H. U. Lee, E. S. Park, S. C. Lee, J.-W. Lee, S. W. Jeong, C. H. Kim, Y.-C. Lee, Y. S. Huh and J. Lee, *ACS Appl. Mater. Interfaces*, 2014, **6**, 3365–3370.
121 P. Pandya, T. J. Webster and S. Ghosh, *Front. Chem.*, 2024, **12**, 1458804.
122 P. Zhu, X. Zhao, Q. Zhu, X. Han, Y. Tang, S. Liao, Z. Gao, Z. Wang, W. Bi, Q. Xu, L. Zhang and M. Xu, *Chem. Eng. J.*, 2023, **470**, 144042.
123 P. Zhu, Y. Liu, Y. Tang, S. Zhu, X. Liu, L. Yin, Q. Liu, Z. Yu, Q. Xu, D. Luo and J. Wang, *Chin. Chem. Lett.*, 2024, **35**, 108689.
124 J. Liu, X. Ma, S. Jin, X. Xue, C. Zhang, T. Wei, W. Guo and X.-J. Liang, *Mol. Pharmaceutics*, 2016, **13**, 1723–1730.
125 X. Xue, Y. Zhao, L. Dai, X. Zhang, X. Hao, C. Zhang, S. Huo, J. Liu, C. Liu, A. Kumar, W.-Q. Chen, G. Zou and X.-J. Liang, *Adv. Mater.*, 2014, **26**, 712–717.
126 J. Wang, J. Bhattacharyya, E. Mastria and A. A. Chilkoti, *J. Controlled Release*, 2017, **260**, 100–110.
127 J. Pilch, E. Matysiak-Brynda, A. Kowalczyk, P. Bujak, Z. Mazerska, A. M. Nowicka and E. E. Augustin, *ACS Appl. Mater. Interfaces*, 2020, **12**, 17276–17289.
128 J. Pilch, P. Kowalik, P. Bujak, A. M. Nowicka and E. Augustin, *Nanomaterials*, 2021, **11**, 462.

129 Q. Wang, X. Huang, Y. Long, X. Wang, H. Zhang, R. Zhu, L. Liang, P. Teng and H. Zheng, *Carbon*, 2013, **59**, 192–199.
130 H. U. Lee, S. Y. Park, B. Son, S. C. Lee, J. W. Lee, Y.-C. Lee, K. S. Kang, M. I. Kim, H. G. Park, S. Choi, Y. S. Huh, S.-Y. Lee, K.-B. Lee, Y.-K. Oh and J. Lee, *Sci. Rep.*, 2014, **4**, 4665.
131 X. Cai, Y. Luo, W. Zhang, D. Du and Y. Lin, *ACS Appl. Mater. Interfaces*, 2016, **8**, 22442–22450.
132 P. Sadhukhan, M. Kundu, S. Chatterjee, N. Ghosh, P. Manna, J. Das and P. C. Sil, *Mater. Sci. Eng., C*, 2019, **100**, 129–140.
133 H. Chen, B. Li, M. Zhang, K. Sun, Y. Wang, K. Peng, M. Ao, Y. Guo and Y. Gu, *Nanoscale*, 2014, **6**, 12580–12590.
134 F. D. Duman, I. Hocaoglu, D. G. Ozturk, D. Gozuacik, A. Kiraz and H. Y. Acar, *Nanoscale*, 2015, **7**, 11352–11362.
135 C. Guihua, C. Wenjie, W. Zhuang, Y. Renxu, L. Hua, G. Jinming and S. Xintao, *Biomaterials*, 2009, **30**, 1962–1970.
136 F. D. Duman, Y. Akkoc, G. Demirci, N. Bavili, A. Kiraz, D. Gozuacik and H. Y. Acar, *J. Mater. Chem. B*, 2019, **7**, 7363–7376.
137 M. Hashemkhani, G. Demirci, A. Bayir, A. Multi, A. Sennaroglu, L. M. Hadi, E. Yaghini, M. Loizidou, A. J. MacRobert and H. Y. Acar, *Nanoscale*, 2021, **13**, 14879–14899.
138 B. Krammer and K. Plaetzer, *Photochem. Photobiol. Sci.*, 2008, **7**, 283–289.
139 A. Di Martino, A. Pavelkova, P. S. Postnikov and V. Sedlarik, *J. Photochem. Photobiol., B*, 2017, **175**, 226–234.
140 A. A. P. Mansur, M. R. B. Paiva, O. A. L. Cotta, L. M. Silva, I. C. Carvalho, N. S. V. Capanema, S. M. Carvalho, E. A. Costa, N. R. Martin, R. Ecco, B. S. Santos, S. L. Fialho, Z. I. P. Lobato and H. S. Mansur, *Int. J. Biol. Macromol.*, 2022, **210**, 530–544.
141 Q. Gong, T. Zhu, L. Zhang, H. Wu, Y. Miao and Y. Hu, *Discover Oncol.*, 2025, **16**, 538.
142 E. Matysiak-Brynda, P. Bujak, E. Augustin, A. Kowalczyk, Z. Mazerska, A. Pron and A. M. Nowicka, *Nanoscale*, 2018, **10**, 1286–1296.
143 M. Ruzycka-Ayoush, P. Kowalik, A. Kowalczyk, P. Bujak, A. M. Nowicka, M. Wojewodzka, M. Kruszewski and I. Grudzinski, *Cancer Nanotechnol.*, 2021, **12**, 8.
144 J. Pilch, P. Kowalik, A. Kowalczyk, P. Bujak, A. Kasprzak, E. Paluszkiewicz, E. Augustin and A. M. Nowicka, *Int. J. Mol. Sci.*, 2022, **23**, 1261.
145 J. Pilch, A. Potęga, A. Kowalczyk, A. Kasprzak, P. Kowalik, P. Bujak, E. Paluszkiewicz, E. Augustin and A. M. Nowicka, *Pharmaceutics*, 2023, **15**, 201.
146 J. Pilch, A. Potęga, P. Kowalik, A. Kowalczyk, P. Bujak, A. Kasprzak, E. Paluszkiewicz and A. M. Nowicka, *Pharmacol. Rep.*, 2024, **76**, 823–837.
147 M. Zheng, S. Liu, J. Li, D. Qu, H. Zhao, X. Guan, X. Hu, Z. Xie, X. Jing and Z. Sun, *Adv. Mater.*, 2014, **26**, 3554–3560.
148 M. Zheng, Z. Xie, D. Qu, D. Li, P. Du, X. Jiang and Z. Sun, *ACS Appl. Mater. Interfaces*, 2013, **5**, 13242–13247.
149 D. Qu, M. Zheng, P. Du, Y. Zhou, L. Zhang, D. Li, H. Tan, Z. Zhao, Z. Xie and Z. Sun, *Nanoscale*, 2013, **5**, 12272–12277.
150 S. N. Baker and G. A. Baker, *Angew. Chem., Int. Ed.*, 2010, **49**, 6726–6744.
151 L. Yang, W. Jiang, L. Qiu, X. Jiang, D. Zuo, D. Wang and L. Yang, *Nanoscale*, 2015, **7**, 6104–6113.
152 L. Yang, Z. Wang, J. Wang, W. Jiang, X. Jiang, Z. Bai, Y. He, J. Jiang, D. Wang and L. Yang, *Nanoscale*, 2016, **8**, 6801–6809.
153 L. Cheng, Y. Li, X. Zhai, B. Xu, Z. Cao and W. Liu, *ACS Appl. Mater. Interfaces*, 2014, **6**, 20487–20497.
154 X. Gao, Y. Cui, R. M. Levenson, L. W. K. Chung and S. Nie, *Nat. Biotechnol.*, 2004, **22**, 969–976.
155 Z. Xu, Y. Feng, X. Liu, M. Guan, C. Zhao and H. Zhang, *Colloids Surf., B*, 2010, **81**, 503–507.
156 J. D. Lunn and D. F. Shantz, *Chem. Mater.*, 2009, **21**, 3638–3648.
157 K. M. Huh, J. Hashi, T. Ooya and N. Yui, *Macromol. Chem. Phys.*, 2000, **201**, 613–619.
158 Z. Xu, B. Li, W. Tang, T. Chen, H. Zhang and Q. Wang, *Colloids Surf., B*, 2011, **88**, 51–57.
159 J. A. Luckanagul, C. Pitakchatwong, P. R. N. Bhuket, C. Muangnoi, P. Rojsitthisak, S. Chirachanchai, Q. Wang and P. Rojsitthisak, *Carbohydr. Polym.*, 2018, **181**, 1119–1127.
160 A. S. Patil, A. P. Gadad, R. D. Hiremath and P. M. Dandagi, *J. Polym. Environ.*, 2018, **26**, 596–606.
161 Z. Ranjbar-Navazi, M. Fathi, E. D. Abdolahinia, Y. Omidi and S. Davaran, *Mater. Sci. Eng., C*, 2021, **118**, 111469.
162 L. Tan, R. Huang, X. Li, S. Liu, Y.-M. Shen and Z. Shao, *Carbohydr. Polym.*, 2017, **157**, 325–334.
163 G. Prencipe, S. M. Tabakman, K. Welsher, Z. Liu, A. P. Goodwin, L. Zhang, J. Henry and H. Dai, *J. Am. Chem. Soc.*, 2009, **131**, 4783–4787.
164 F. Hu, C. Li, Y. Zhang, M. Wang, D. Wu and Q. Wang, *Nano Res.*, 2015, **8**, 1637–1647.
165 H. Uludag, *Curr. Pharm. Des.*, 2002, **8**, 1929–1944.
166 C. Li, Y. Zhang, G. Chen, F. Hu, K. Zhao and Q. Wang, *Adv. Mater.*, 2017, **29**, 1605754.
167 X. Hao, C. Li, Y. Zhang, H. Wang, G. Chen, M. Wang and Q. Wang, *Adv. Mater.*, 2018, **30**, 1804437.
168 P.-J. Wu, K.-L. Ou, J.-K. Chen, H.-P. Fang, S.-H. Tzing, W.-X. Lin and J.-Y. Chang, *Mater. Lett.*, 2014, **128**, 412–416.
169 S. Ling, X. Yang, C. Li, Y. Zhang, H. Yang, G. Chen and Q. Wang, *Angew. Chem., Int. Ed.*, 2020, **59**, 7219–7223.
170 C. Ding, X. Cao, C. Zhang, T. H. N. Hua and Y. Xian, *Nanoscale*, 2017, **9**, 14031–14038.
171 M. Tian, S. Tatsuura, M. Furuki, Y. Sato, I. Iwasa and L. S. Pu, *J. Am. Chem. Soc.*, 2003, **125**, 348–349.
172 S. Li, Q. Zou, R. Xing, T. Govindaraju, R. Fakhrullin and X. Yan, *Theranostics*, 2019, **9**, 3249–3261.
173 S. Li, Q. Zou, Y. Li, C. Yuan, R. Xing and X. Yan, *J. Am. Chem. Soc.*, 2018, **140**, 10794–10802.

174 R. Liu, R. Xing, Q. Zou, G. Ma, H. Möhwald and X. Yan, *Angew. Chem., Int. Ed.*, 2016, **55**, 3036–3039.
175 E. Laviron, R. Meunier-Prest and R. Lacasse, *J. Electroanal. Chem.*, 1994, **375**, 263–274.
176 C. G. R. Heald, G. G. Wildgoose, L. Jiang, T. G. J. Jones and R. G. Compton, *ChemPhysChem*, 2004, **5**, 1794–1799.
177 Ch. A. Thorogood, G. G. Wildgoose, T. G. J. Jones and R. G. Compton, *New J. Chem.*, 2007, **31**, 958–965.
178 D. Wen, N. Kirkwood and P. Mulvaney, *J. Phys. Chem. Lett.*, 2023, **14**, 3669–3676.
179 A. S. Portniagin, S. P. Karamysheva, K. V. Bogdanov, E. V. Ushakova and A. L. Rogach, *Nanoscale*, 2025, **17**, 16193–16212.
180 M. Le Goas, J. Saber, S. G. Bolívar, J.-M. Rabanel, J.-M. Awogni, D. C. Boffito and X. Banquy, *Nano Today*, 2022, **45**, 101516.